



USE OF GENETIC ALGORITHMS IN THE OPTIMIZATION
FREE RADICAL POLYMERIZATIONS EXHIBITING
THE TROMMSDORFF EFFECT

A Thesis Submitted
in Partial Fulfillment of the Requirements
for the Degree of
Master of Technology

by
S.S.S. Chakravarthy

to the
DEPARTMENT OF CHEMICAL ENGINEERING
INDIAN INSTITUTE OF TECHNOLOGY, KANPUR

March 1996.

13 MAY 1986
CENTRAL LIBRARY
CANTON
Doc. No. A. 121485

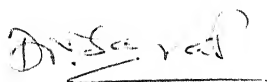
CHE-1986-M-CHA-USE



A121485

CERTIFICATE

This is to certify that the present work entitled, USE OF GENETIC ALGORITHMS IN THE OPTIMIZATION OF FREE RADICAL POLYMERIZATIONS EXHIBITING THE TROMMSDORFF EFFECT, by *S.S.S. Chakravarthy* has been carried out under our supervision and that this work has not been submitted elsewhere for a degree.

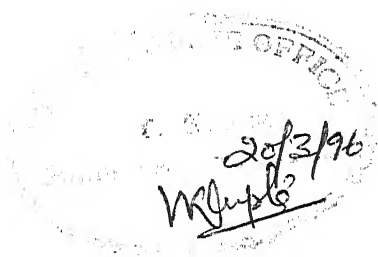


Prof. D.N. Saraf,
Professor,
Department of Chemical Engineering,
IIT, Kanpur.



Prof. S.K. Gupta,
Professor,
Department of Chemical Engineering,
IIT, Kanpur.

March, 1996



ABSTRACT

The genetic algorithm (GA) is adapted and used to obtain optimal temperature histories for methyl methacrylate polymerizations. The reaction time is minimized, while simultaneously requiring the attainment of design values of the final monomer conversion and number average chain length. The technique is robust, and gives near-global-optimal solutions. As such, it can easily be used for on-line optimizing control of free radical polymerization reactors in which the reaction is associated with the Trommsdorff effect. The results obtained from GA can be improved further if these are provided as initial guesses to a computer code using the Pontryagin's minimum principle with the first order control vector iteration method.

ACKNOWLEDGEMENTS

In retrospect, I feel that its been a good decision joining M.Tech here at IIT. Kanpur. Its indeed my pleasure to acknowledge the memorable moments I had here.

To begin with I consider myself fortunate for having got the opportunity to work under some excellent guidance, the guidance of Prof. S.K. Gupta and Prof. D.N. Saraf. Its their constant encouragement and the stimulating research environment provided by them that made me always relish some unknown pleasure out of working. To be candid, I am at dearth of words to express my feelings of gratitude towards them. Truely, to both I owe a timeless debt.

I take this opportunity to express my sincere thanks to Prof. Kalyanmoy Deb for providing valuble suggestions which proved very fruitful towards the end.

Its my pleasure to thank all my friends, Sastry "Kukka", Poorna "Mr. Singh", Bhargav "Bull", Anil "A - Howle", Murthy "Basu", Vasant "Rayadu", Vidyanath "Vidya", C.S. Rao "Chemeta", Kaliprasad "Kali", Harikishan Reddy, Bandaru "Band", Chender "Tender", 'Ritwik "A-be", Rajiv, and above all my dear brother Prasad "Mr. Cool", for making my stay here a real memorable one.

I thank all my labmates Dua, sareen, Seth, Kohli, Verma, Sajith, Mankar, Pallav, Kishlay, for their kind cooperation.

Finally, to my parents and my sisters go my eternal gratitude for their constant love and support.

S.S.S. Chakravarthy

CONTENTS

| | | |
|-----------------|-------------------------------|-------|
| CERTIFICATE | | (i) |
| ABSTRACT | | (ii) |
| ACKNOWLEDGEMENT | | (iii) |
| LIST OF FIGURES | | (iv) |
| LIST OF TABLES | | (vi) |
| NOMENCLATURE | | (vii) |
| CHAPTER 1 | INTRODUCTION | 1 |
| CHAPTER 2 | FORMULATION | 8 |
| CHAPTER 3 | RESULTS AND DISCUSSION | 23 |
| CHAPTER 4 | CONCLUSIONS , ACKNOWLEDGEMENT | 48 |
| CHAPTER 5 | SUGGESTIONS FOR FUTURE WORK | 49 |
| REFERENCES | | 50 |
| APPENDIX A | ADDITIONAL RESULTS | 53 |
| APPENDIX B | ADDITIONAL TABLES | 66 |
| APPENDIX C | COMPUTER PROGRAMS | 73 |

LIST OF FIGURES

| FIGURE | TITLE | PAGE |
|--------|--|------|
| 1 | Flow chart indicating the working of GA. | 12 |
| 2 | $x_m(t)$ (solid) and $\mu_n(t)$ (dotted) for isothermal bulk polymerization of MMA using AIBN ($[I]_0 = 25.8 \text{ mol/m}^3$). | 24 |
| 3 | Evolution of temperature histories towards the optimal one, with generation number, N_g , corresponding to $x_{md} = 0.94$, $\mu_{nd} = 1800$ (for parameters of Table 5). Arrows indicate the end points of corresponding curves. | 26 |
| 4 | $\mu_n(t)$ corresponding to $T_{opt}(t)$ for the GA15 run, as well as for those corresponding to Fig. 6. | 27 |
| 5 | $x_m(t)$ corresponding to the GA15 run, as well as for those given in Fig. 6. | 28 |
| 6 | $T_{opt}(t)$ corresponding to the conditions of Fig. 3 using the P1 (dotted) and GA (solid) techniques. GA15 corresponds to the reference run (Table 5) while GA30 corresponds to $[\Delta T_{min}, \Delta T_{max}] = \pm 30^\circ\text{C}$ (all other parameters same as given in the Table 5). Arrow indicates t_f for P1. | 31 |
| 7 | $T_{opt}(t)$ obtained with the P1 (dotted) technique using the optimal history from GA15 (solid) as an initial guess. | 33 |

- 8 Effect of varying N_p and N_{str} on the optimal temperature histories. Curve 1: $N_p = 50$; curve 2: $N_p = 200$; curve 3: $N_{str} = 14$. Results for the reference run (GA15) also shown for comparison. 36
- 9 Effect of varying N_{ga} on the optimal temperature history. Curve 4: $N_{ga} = 20$; curve 5: $N_{ga} = 30$. 38
- 10 Effect of varying p_m , p_c , N_{sim} and RS on the optimal temperature history. Curve 6: $p_m = 10^{-5}$; curve 7: $p_c = 0.98$; curve 8: $N_{sim} = 80$. 39
- 11 Effect of varying $[\Delta T_{min}, \Delta T_{max}]$ and S on the optimal temperature history. Curves 10 and 11: $[\Delta T_{min}, \Delta T_{max}] = \pm 20$ and $\pm 30^\circ\text{C}$ respectively. Curve 12: $S = 0.4$. 40
- 12 Effect of varying x_{md} on the optimal temperature histories. Curve 13 corresponds to $x_{md} = 0.95$. 42
- 13 Effect of varying μ_{nd} and $[I]_0$ on the optimal temperature histories. Curves 14 and 15: $\mu_{nd} = 1600$ and 2000, respectively; curve 16: $[I]_0 = 15.48 \text{ mol/m}^3$. 43
- 14 $\mu_n(t)$ corresponding to the optimal temperature histories given in Fig. 13. 44
- 15 Variation of the polydispersity index (PDI) with time. The solid curve represents the PDI corresponding to the GA15 run, while the dotted curves correspond to isothermal polymerizations at 80°C and 90°C . 47

LIST OF TABLES

| TABLE | TITLE | PAGE |
|-------|---|------|
| 1 | Kinetic scheme for Polymerization of MMA. | 2 |
| 2 | Decoding and Adaptive mapping procedure for $N_{ga} = 2$. | 16 |
| 3 | Formulation of the optimal control problem using Pontryagin's minimum principle with first order control vector iteration method. | 21 |
| 4 | Parameters used for Reference run. | 29 |
| 5 | Some details corresponding to $T_{opt}(t)$ shown in Figs. 8-14. | 35 |

NOMENCLATURE

| | |
|--|--|
| a | lower limit of u |
| b | upper limit of u |
| D_n | dead polymer molecule having n repeating units |
| $E_d, E_i, E_f, E_p,$ E_s, E_{tc}, E_{td} | activation energies for the reactions in Table 1, kJ mol^{-1} |
| f | initiator efficiency |
| f_o | initiator efficiency in the limiting case of zero diffusional resistance |
| F | fitness function (Eq. 11) |
| I | objective function |
| I | moles of initiator at any time t , mol |
| $[I]_o$ | initial molar concentration of initiator, mol m^{-3} |
| $k_d, k_i, k_f, k_p,$ k_s, k_{tc}, k_{td} | rate constants for the reactions in Table 1 at any time t , s^{-1} or $\text{m}^3 \text{mol}^{-1} \text{s}^{-1}$ |
| $k_{p,o}, k_{i,o}$ $k_{tc,o}, k_{td,o}$ | intrinsic (in absence of cage, gel and glass effects) rate constants, $\text{m}^3 \text{mol}^{-1} \text{s}^{-1}$ |
| $k_t, k_{t,o}$ | $k_{tc} + k_{td}; k_{tc,o} + k_{td,o}$ |
| $k_d^o, k_{p,o}^o, k_{td,o}^o$ | frequency factors for intrinsic rate constants, s^{-1} or $\text{m}^3 \text{mol}^{-1} \text{s}^{-1}$ |
| $l_{N_{\text{chr}}}^{(i)}$ | i^{th} chromosome in population |
| M | moles of monomer in liquid phase, mol |
| M_{jp} | molecular weight of the polymer jumping unit, kg mol^{-1} |

| | |
|--------------------------|--|
| M_n | number average molecular weight = $(MW_m)(\lambda_1 + \mu_1) / (\lambda_o + \mu_o)$, kg mol ⁻¹ |
| M_w | weight average molecular weight = $(MW_m)(\lambda_2 + \mu_2) / (\lambda_1 + \mu_1)$, kg mol ⁻¹ |
| $(MW_I), (MW_m), (MW_s)$ | molecular weights of pure primary radicals, monomer and solvent, kg mol ⁻¹ |
| N_{chr} | total number of binary digits in chromosome = $N_{ga} N_{str}$ |
| N_g | generation number |
| N_{ga} | number of u values GA generates |
| N_p | number of chromosomes in the population |
| N_{sim} | number of u values after interpolation |
| N_{str} | number of binary digits representing each of the N_{ga} control variables |
| \vec{p} | vector representing the model parameters $\theta_f, \theta_p, \theta_t$ |
| p_c | probability for crossover |
| p_m | probability for mutation |
| PDI | polydispersity index (= M_w/M_n) |
| P_n | growing polymer radical having n repeat units |
| R | primary radical |
| R_{li}, R_{lm}, R_{ls} | rate of continuous addition of (liquid) initiator, monomer, or solvent to reactor, mol s ⁻¹ |
| R_{vm}, R_{vs} | rate of evaporation of monomer or solvent, mol s ⁻¹ |
| RS | parameter in random generator code |
| S | moles of solvent in liquid phase, mol |
| S | safety factor |

| | |
|--|--|
| S^\cdot | solvent radical |
| t | time, s |
| t_f | total (final) reaction time, s |
| t_{fo} | initially assumed value for t_f , s |
| $T^{(0)}(t)$ | initial guess temperature history in Pontryagin's technique |
| $T(t)$ | temperature at time t , K |
| u | control vector (scalar, u , in this work) |
| $\tilde{u}^{(i)}(j)$ | value of control variable at the end of j^{th} time interval in the i^{th} chromosome |
| u_{\min}, u_{\max} | lower and upper bounds on the control variable |
| $\Delta u_{\min}, \Delta u_{\max}$ | minimum and maximum changes allowed between neighboring values of u |
| $U^{(i)}(j)$ | value of control variable at the end of j^{th} (interpolated) time interval in the i^{th} chromosome |
| V_l | volume of liquid at time t , m^3 |
| V_{fm}, V_{fs}, V_{fp} | free volumes of monomer, solvent, polymer |
| $\hat{V}_I^*, \hat{V}_m^*, \hat{V}_s^*, \hat{V}_p^*$ | specific critical hole free volumes of initiator, monomer, solvent and polymer, m^3/kg |
| w_1, w_2 | weightage factors |
| \mathbf{x} | vector representing state variables |
| $\tilde{x}_m(t)$ | monomer conversion (molar) at time t (Eq. 7a) |

Greek Letters

| | |
|--------------------------------|---|
| ξ_{I3}, ξ_{13} | parameters in gel effect model (defined in Ref. 19) |
| ζ_m, ζ_{m_1} | net monomer added to the reactor, as defined in Ref. 19 |
| $\theta_f, \theta_p, \theta_t$ | adjustable parameters in the model for cage, gel and glass effects, respectively, $m^3 \text{ mol}^{-1}$, s, s |
| λ_k | kth ($k=0,1,2,\dots$) moment of live (P_n) polymer radicals $\equiv \sum_{n=1}^{\infty} n^k P_n$, mol |
| μ_k | kth ($k=0,1,2,\dots$) moment of dead (D_n) polymer chains $\equiv \sum_{n=1}^{\infty} n^k D_n$, mol |
| μ_n | number average chain length at time t $\equiv (\lambda_1 + \mu_1) / (\lambda_0 + \mu_0)$ |
| μ_w | weight average chain length at time t $\equiv (\lambda_2 + \mu_2) / (\lambda_1 + \mu_1)$ |
| $\xi_{13}, \xi_{23}, \xi_{I3}$ | ratio of the molar volume of the monomer, solvent, and initiator jumping unit to the critical molar volume of the polymer, respectively |
| ρ_m, ρ_p, ρ_s | density of pure (liquid) monomer, polymer or solvent at temperature T (at time t), kg m^{-3} |
| ϕ_m, ϕ_p, ϕ_s | volume fractions of monomer, polymer or solvent in liquid at time t |
| ψ, ψ_{ref} | defined in Table A3 |

Subscripts/Superscripts

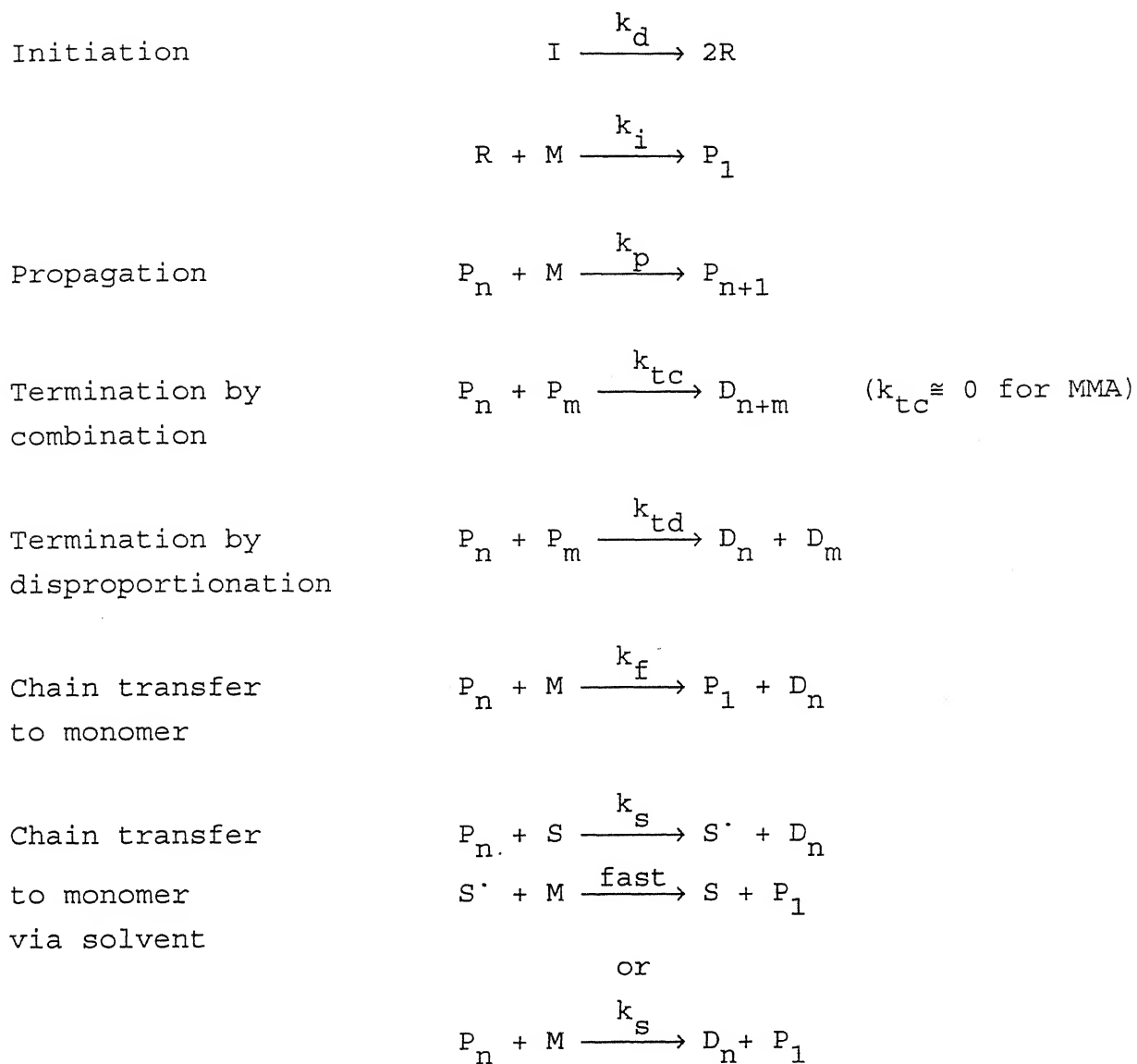
| | |
|-----|-----------------------------|
| d | desired value |
| f | final value (at $t = t_f$) |
| min | minimum |
| o | initial value |
| opt | optimal value |

CHAPTER 1

INTRODUCTION

A considerable amount of research has been reported in the last several years on the modeling and optimization of free radical polymerizations exhibiting the gel or Trommsdorff effect^{1,2}. The various models have been reviewed by O'Driscoll³ and Hamielec⁴ and more recently by Achilias and Kiparissides^{5,6} and by Mita and Horie⁷. These models have been used in several optimization studies which have been reviewed by Farber⁸ as well as by Louie and Soong⁹. Yet, there are several unanswered questions. For example, Faldi et al.^{10,11} have measured the diffusion coefficients of methyl methacrylate (MMA) and other model compounds in MMA - polymethyl methacrylate (PMMA) systems using forced Rayleigh scattering and field-gradient NMR, and have inferred that the propagation rate constant, k_p (see Table 1 for kinetic scheme), is not diffusion controlled, contrary to the general assumption used in almost all theories. They claim that the decrease in k_p with increasing monomer conversion (x_m), which is necessary to fit experimental data on the rates of polymerization, needs an explanation different from the one traditionally being offered. Russell, Gilbert and coworkers¹²⁻¹⁴ are developing improved theories along similar lines. However, the earlier theories are fairly good and are still being used to

TABLE 1
KINETIC SCHEME FOR POLYMERIZATION OF MMA



model, optimize and control industrial reactors, even though they are semi-empirical in nature.

One group of these theories has originated from the molecular theory of Chiu et al.¹⁵ Chiu et al. relate the decrease of the rate constants, k_p and k_t , to the polymer concentration and the average molecular weight (the latter, through the initial concentration, $[I]_0$, of the initiator) at any time, t . Achilias and Kiparissides^{5,6} related some of the parameters of this early model to quantities which could be measured directly using non-polymerizing systems. There was only a single curve-fit parameter, j_{co} , in their model, which was correlated to the initial value of the number average chain length, μ_{no} . The qualitative trends of the experimental data on the isothermal polymerization of MMA in small ampoules^{16,17} (namely, sharp increase in x_m and the weight average chain length, μ_w , with t , after the onset of the Trommsdorff effect, and the reaction stopping short of complete monomer conversion even though the reactions are irreversible, the latter being referred to as the glass effect) were well explained by this theory, while quantitative agreement was ensured by curve-fitting the value of the parameter. One major drawback of these versions of this group of theories^{5,6,15} was that they could not be applied to semibatch reactors, or to reactors operating under non-isothermal conditions, and so were of little use in industry where such operations were routinely encountered. Recently, Ray et al.¹⁸ and

Seth and Gupta¹⁹ have presented a theory which relates the rate constants (as well as initiator efficiency¹⁹, f) to the *current* values of the number average chain length, μ_n . The parameters of this theory, θ_f , θ_p , and θ_t (all functions of temperature, T) have been estimated¹⁹ for MMA polymerization using the experimental data of Schulz and Harborth¹⁶ and Balke and Hamielec¹⁷, under *isothermal* conditions in *small* ampoules. The theory so 'tuned' has been able to explain *quantitatively*, experimental data on MMA polymerization in a 1-liter PC-interfaced, stainless steel, Parr[®] reactor using idealized conditions mimicking industrial operations (namely, step changes in temperature²⁰ and step increases in the initiator and monomer concentrations²¹). No additional retuning of the parameters was found to be necessary. This suggests that the theory reflects all the physico-chemical phenomena associated with polymerization quite well. It is to be noted that other groups of theories could have been modified suitably to apply to industrial systems, but it is well recognized²² that almost all theories are about equally successful in explaining rate data and so the use of the relatively simple and continuous models in the group originating from Chiu et al.¹⁵, is justified.

In this work, the recent theory^{18,19} for MMA polymerization has been used to study the optimization of a batch reactor. A commonly studied problem^{8,9} is to obtain the temperature history, $T(t)$ (the control variable), which minimizes the total reaction time, t_f , while simultaneously requiring the

final monomer conversion, x_{mf} , and the final value of the number average chain length, μ_{nf} , to meet certain specifications (called 'desired' values, x_{md} and μ_{nd}). This ensures economic operation as well as product property requirements, and is referred to as the minimum-time problem⁸. A newly emerging technique, called genetic algorithm (GA)²³⁻²⁵, is used to obtain optimal solutions. This is an extremely robust technique and gives solutions which are quite close to *global* optima reasonably fast. Hence, this technique, coupled with a model which is applicable for industrial reactors, is well suited for use for on-line optimizing control of large scale MMA polymerizations (or of other similar free radical polymerizations), provided we can estimate the 'state' of the system on-line. Current experimental work along these lines is in progress, in which the viscosity of the reaction mass is used to estimate the state of the system using inferential²⁶ state variable estimation²⁷. GA is then used to predict the future control action (temperature is being used as the control variable) on a supervisory-level or 'master' PC-AT, and then a 'slave' PC-AT implements this on a 1-liter reactor. To the best of our knowledge, the use of GA for predicting optimal temperature histories has not been reported for any system in the open literature on polymer reaction engineering, nor has GA been used for carrying out an optimally controlled polymerization experimentally. Most of the earlier works⁸ on the optimization of polymerization reactors use the far less robust Pontryagin's

minimum principle²⁷⁻³⁰, or the constrained pattern search technique⁹, to solve a variety of optimization problems as described in the review of Farber⁸, using temperature or initiator addition rates as control variables. These techniques are not suitable for use for on-line optimization work. GA, on the other hand, is a new and extremely powerful search technique based on the mechanics of natural genetics and natural selection. This algorithm was introduced in the mid sixties by Holland²³ and a discussion of the technique and its adaptations, as well as its major applications are available in several books^{24,25}. It involves a random search over the control variable domain after the problem has been appropriately 'coded', usually in terms of 'strings' or 'chromosomes' comprising of binary numbers. The best few solutions 'evolve' over 'generations' using techniques which mimic genetic evolution (hence the name). This new technique has been proved to be very efficient, specially in cases where the objective function is flat and exhibits several local optima. The advantage of GA lies in the fact that it works without requiring much information about the system, in contrast to the traditional techniques which need gradients, initial guesses, etc. Hence, for more complex systems where the gradients cannot be easily evaluated and the initial guess becomes crucial, GAs lead to solutions which are very close to the global optima, or in fact, provide very good initial points to start off other techniques which require excellent initial guesses (e.g., Pontryagin's

minimum principle using the first order control vector iteration method).

CHAPTER 2

FORMULATION

Table 1 gives the kinetic scheme for MMA polymerization (with $k_{tc} \approx 0$). The mass balance equations for MMA polymerization in a semi-batch reactor are given by equations having the general form

$$\frac{d\mathbf{x}}{dt} = \mathbf{F}(\mathbf{x}, \mathbf{u}); \quad \mathbf{x}(t=0) = \mathbf{x}_0 \quad (1)$$

where $\mathbf{x}(t)$ is the vector of state variables defined by

$$\mathbf{x} = [I, M, R, S, \lambda_0, \lambda_1, \lambda_2, \mu_0, \mu_1, \mu_2, \zeta_m, \zeta_{m1}]^T \quad (2)$$

and $\mathbf{u}(t)$ is the vector of control variables [in the present case it is a scalar, $T(t)$]

$$\mathbf{u}(t) = u(t) = T(t) \quad (3)$$

λ_k and μ_k ($k = 0, 1, 2, \dots$) represent the k^{th} moments of the chain length distributions of species P_n and D_n , respectively. ξ_m , ξ_{m1} are additional variables to account for addition and vaporization of monomer after time $t = 0$, and are useful in the definition of the monomer conversion, x_m , for semibatch reactors. The other symbols are defined in the nomenclature. The exact mass balance and moment equations (functions, \mathbf{F} , in Eq. 1) have been given by Ray et al.¹⁸ as well as by Seth and Gupta¹⁹ (Table B1, Appendix B). These equations involve the several rate constants shown in Table 1, as well as the initiator efficiency, f , which quantifies

the wastage of primary radicals, R , due to reactions not included in Table 1.

The initiator efficiency, f , and the rate constants, k_p and k_{td} , are diffusion controlled and are given by the following equations¹⁹

$$f = f_o \left[1 + \theta_f(T) \frac{M}{V_1} \exp\{ \xi_{I3} (\psi - \psi_{ref}) \} \right]^{-1} = f(\mathbf{x}, u, \mathbf{p}) \quad (4a)$$

$$k_p = \left[\frac{1}{k_{p,o}} + \theta_p(T) \left(\frac{\lambda_o}{V_1} \right) \exp\{ \xi_{13} (\psi - \psi_{ref}) \} \right]^{-1} = k_p(\mathbf{x}, u, \mathbf{p}) \quad (4b)$$

$$k_{td} = \left[\frac{1}{k_{td,o}} + \theta_t(T) \mu_n^2 \left(\frac{\lambda_o}{V_1} \right) \exp(\psi - \psi_{ref}) \right]^{-1} = k_{td}(\mathbf{x}, u, \mathbf{p}) \quad (4c)$$

with

$$\mathbf{p} = [\theta_f, \theta_p, \theta_t]^T \quad (5)$$

In this equation, V_1 is the volume of the (liquid) reaction mass, while ψ and ψ_{ref} are parameters related to the weighted average free volume fraction as well as the molecular weight of the 'jumping' unit of the polymer and are functions of temperature (defined in Table B2). ξ_{I3} and ξ_{13} are related to the ratios of molecular weights of equivalent jumping units, and are constants. The model parameters, θ_f , θ_p and θ_t , have been tuned using the isothermal data of Balke and Hamielec¹⁷ on MMA polymerization in small ampoules (see Table B3 for exact expressions). The model has

been found to be in good agreement with the experimental data on a 1-liter Parr[®] reactor^{20,21}. No retuning of the values of the parameters, \tilde{p} , were found to be necessary.

The objective function, I , used in this study is given by

$$\text{Min } I [u(t)] = t_f + w_1 (1 - x_{mf}/x_{md})^2 + w_2 (1 - \mu_{nf}/\mu_{nd})^2 \quad (6a)$$

subject to (s.t.)

$$\frac{dx}{dt} = F(x, u) \quad (6b)$$

$$u_{\min} \leq u(t) \leq u_{\max} \quad (6c)$$

where

$$x_m(t) \equiv (1 - M/\zeta_{m1}) \quad (7a)$$

$$\mu_n(t) = (\lambda_1 + \mu_1)/(\lambda_0 + \mu_0) \quad (7b)$$

$$x_{mf} = x_m(t_f) \quad (7c)$$

$$\mu_{nf} = \mu_n(t_f) \quad (7d)$$

In Eq. 6, x_{md} and μ_{nd} are the *desired* values of monomer conversion and the number average chain length at $t = t_f$, x_{mf} and μ_{nf} are the *actual* values corresponding to $t = t_f$, and w_1 and w_2 are (large) weightage factors. The choice of the objective function in Eq. 6 minimizes the deviations (due to large values of w_1 and w_2) of x_{mf} and μ_{nf} from their desired values. The form of I used in Eq. 6 in which the end point requirements (constraints) are included as 'penalty functions', is quite popular^{8,25}. The choice, $x_{mf} \approx x_{md}$, forces the amount of unreacted monomer to be small, thus keeping post-reactor separation and recycling costs low. The choice, $\mu_{nf} \approx \mu_{nd}$, forces the polymer properties to be as per specifications

since several physical properties of polymers are related to the value of their μ_n . The objective function in Eq. 6 has been used earlier by Sachs, Lee and Biesenberger³¹ but with a different kinetic model, and by Farber and Laurence³² for styrene polymerization. The initial values, \mathbf{x}_0 in Eq.1 are given by

$$\mathbf{x}_0 = [I_0, M_0, 0, 0, 0, 0, 0, 0, 0, 0, M_0, M_0]^T \quad (8)$$

Fig.1 gives the flow chart illustrating how GA, as applied to the present problem (Eq. 6), works. We have had to make several adaptations to the conventional algorithm^{24,25} and the computer code (SGA²⁵) in order to solve the present problem. Initially (at generation number, $N_g = 0$), a population having N_p chromosomes, $l_{N_{chr}}^{(i)}$; $i = 1, 2, \dots, N_p$, is generated. Each chromosome in this population comprises of a sequence of N_{ga} numbers (called substrings) which are binary representations of values of the control variable at N_{ga} equispaced points in $0 \leq t \leq t_{fo}$ (t_{fo} , an initial estimate of t_f , is to be supplied). Each of these substrings, in turn, comprises of a set of N_{str} binary numbers (0 or 1). Thus, each chromosome has $N_{chr} \equiv N_{ga} N_{str}$ binary digits. The N_{chr} individual binaries are generated using a random number generator subroutine. The binary string (sequence of N_{chr} binaries) of the i^{th} chromosome, when decoded and interpolated (mapped) between the upper ($u \leq b$) and lower ($u \geq a$) bounds of u , gives a digitized u -history (a set of N_{ga} values), $[u^{(i)}] \equiv$

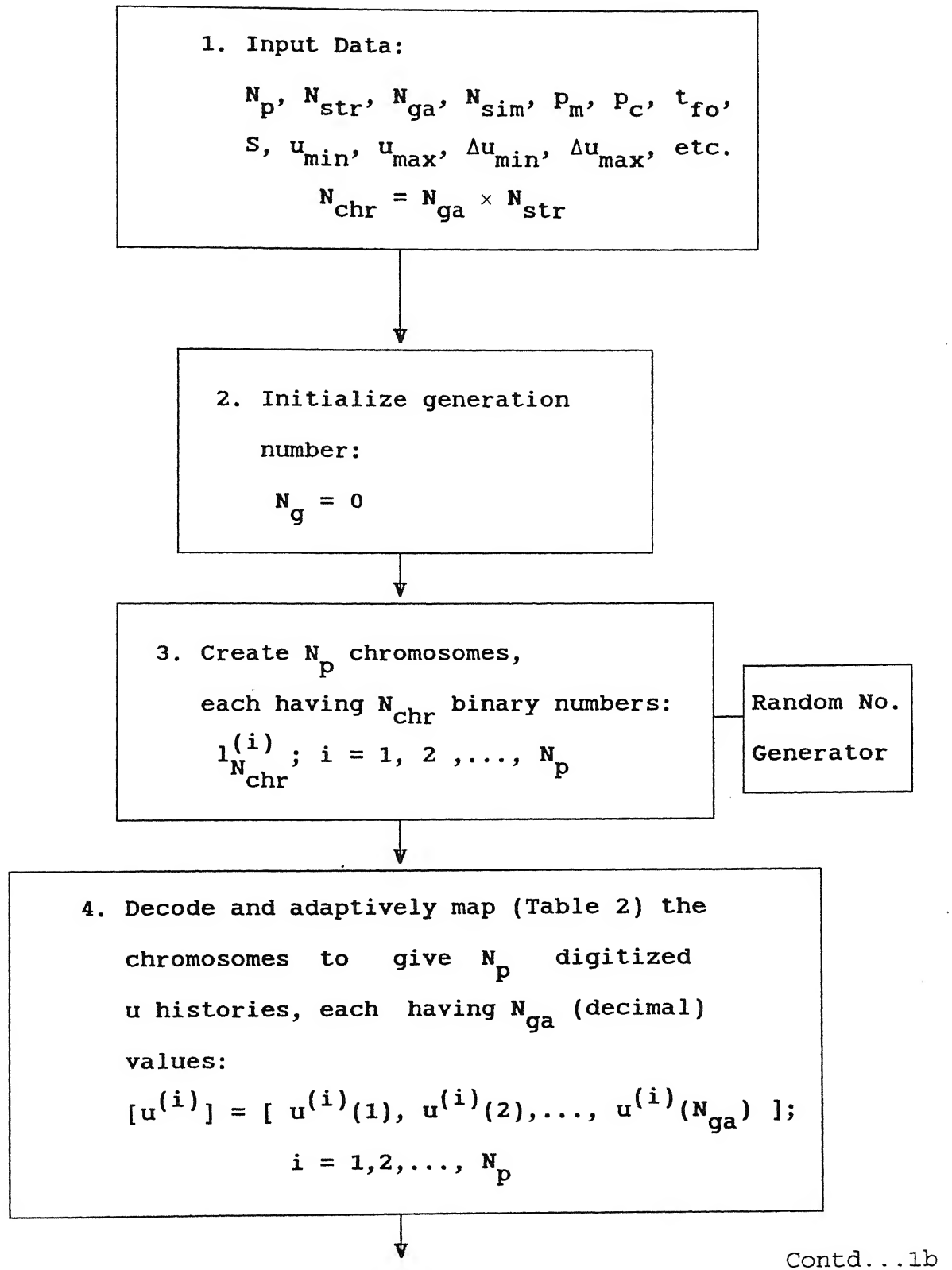
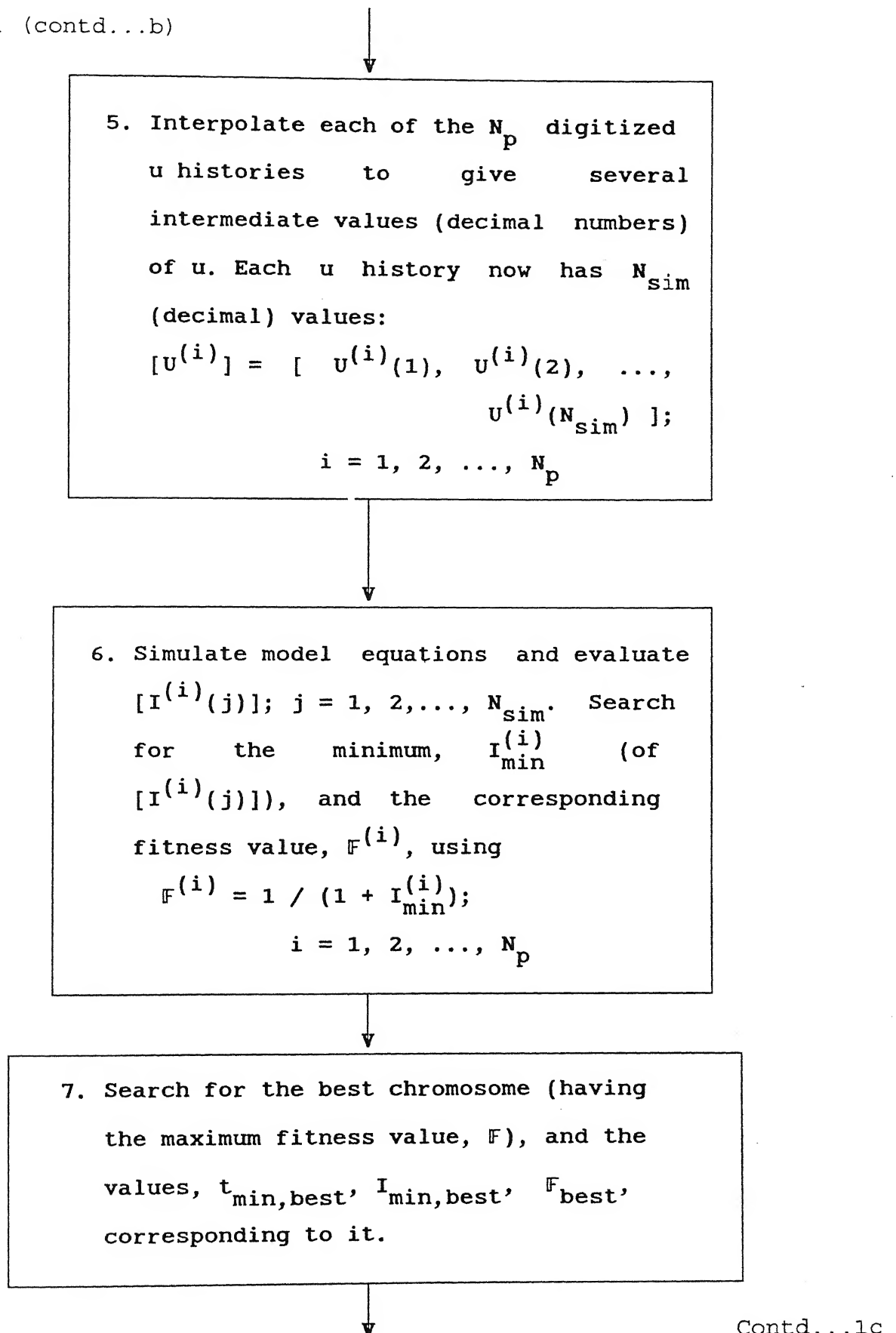


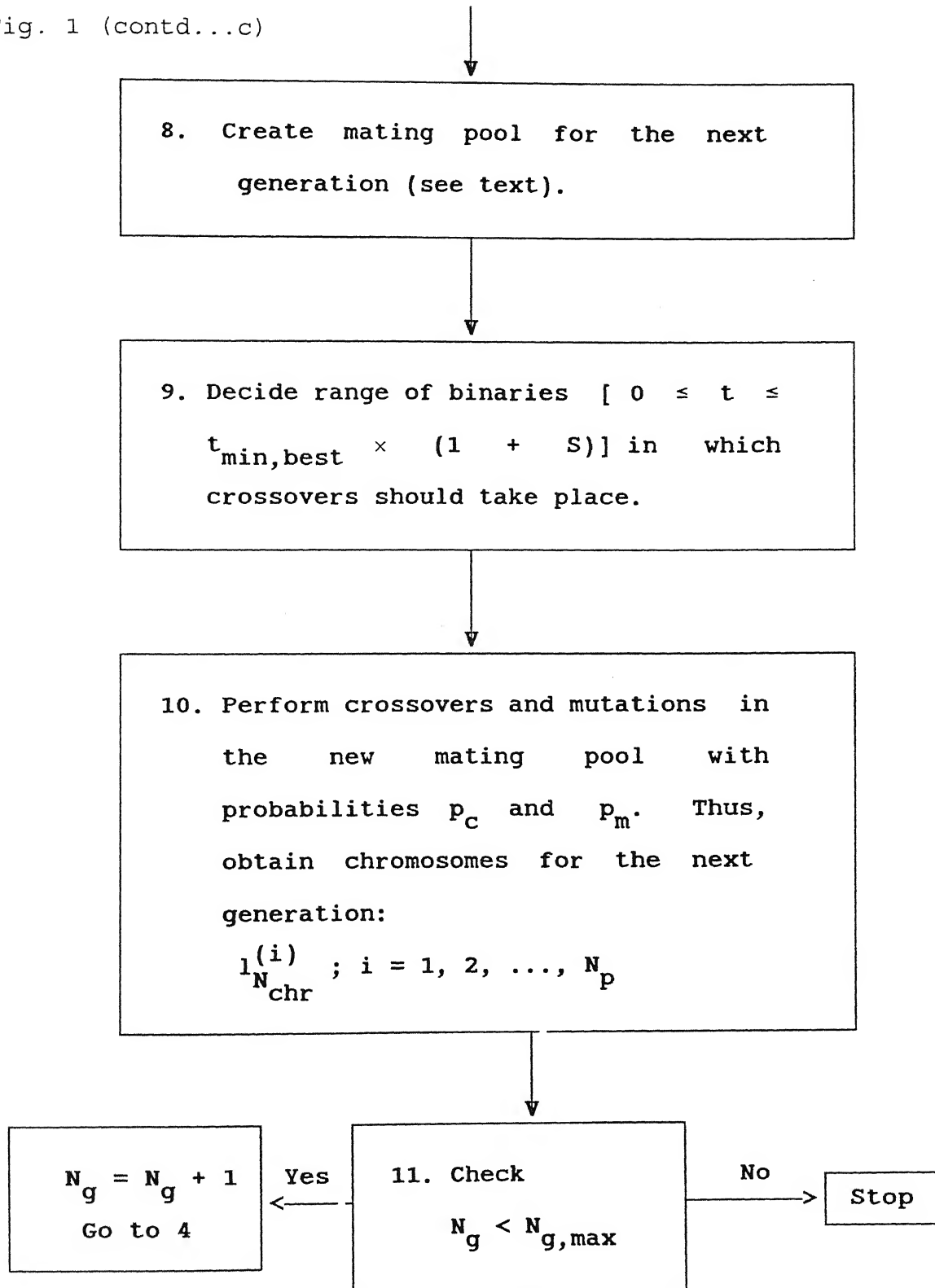
Fig. 1 Flowchart indicating the working of GA.

Fig. 1 (contd...b)



Contd...1c

Fig. 1 (contd...c)



$[u^{(i)}(1), u^{(i)}(2), \dots, u^{(i)}(N_{ga})]$, corresponding to that chromosome, as described in Table 2 (in the conventional GA^{24,25}, $b = u_{\max}$ and $a = u_{\min}$). At this stage we have a set of N_p chromosomes, each representing a different digitized $u(t)$ history, appropriately coded in the form of a string of N_{chr} binaries. It is obvious that the minimum difference between any two digitized values of u is $(b - a)/(2^{N_{str}} - 1)$, this being the accuracy to which u can be determined.

The values of $u^{(i)}(j)$ generated by the above procedure using $b = u_{\max}$ and $a = u_{\min}$, could fluctuate wildly between these two limits. This leads to significant oscillations in the optimal u -histories, and is both undesirable and non-implementable. In order to reduce these oscillations, further constraints are clamped on to the values of $u^{(i)}(j)$ in the present study, so that *neighbouring* values of u do not differ by more than some prescribed values, Δu_{\min} and Δu_{\max} . Thus,

$$\Delta u_{\min} \leq \Delta u^{(i)}(j) [= u^{(i)}(j+1) - u^{(i)}(j)] \leq \Delta u_{\max} \quad (9)$$

or

$$u^{(i)}(j) + \Delta u_{\min} \leq u^{(i)}(j+1) \leq u^{(i)}(j) + \Delta u_{\max} \quad (10)$$

where Δu_{\min} is a negative number. Thus, the first value, $u^{(i)}(1)$, corresponding to $t = 0$, is determined *randomly* to lie between u_{\max} and u_{\min} , while all subsequent values are determined *randomly* within a smaller range around the previous value. This procedure is being called adaptive mapping. The accuracy (minimum

TABLE 2
DECODING AND ADAPTIVE MAPPING PROCEDURE FOR

$$N_{ga} = 2$$

$$N_{chr} = N_{ga} \quad N_{str} = 2N_{str} ; a \leq u \leq b^*$$

Example:

$$\begin{matrix} (i) \\ 1 \\ N_{chr} \end{matrix} = \begin{matrix} [& 10011...0 & ; & 11100...0 &] & ; & i = 1, 2, \dots, N_p \\ & N_{str} \text{ binaries} & & N_{str} \text{ binaries} & \end{matrix}$$

'Decode' each of the (two sets of) binary numbers into decimal numbers, d_1 and d_2 , using, for example,

$$d_1 = 1 \times 2^{N_{str}-1} + 0 \times 2^{N_{str}-2} + \dots + 0 \times 2^0$$

Now, using the 'mapping' obtain the digitized u-history

$$\begin{aligned} [u^{(i)}(j)] &= [u^{(i)}(1), u^{(i)}(2)] \\ &= a + d_j \times VAL \quad ; i = 1, 2, \dots, N_p \\ &\quad j = 1, 2 \end{aligned}$$

where

$$VAL = (b - a) / (2^{N_{str}} - 1)$$

$$\begin{aligned} * a &= u_{min}, b = u_{max} ; \text{ for } j = 1 \\ a &= u^{(i)}(j - 1) + \Delta u_{min}, b = u^{(i)}(j - 1) + \Delta u_{max} ; \\ &\text{for } j > 1; \text{ s.t. } u_{min} \leq a, b \leq u_{max} \end{aligned}$$

difference between values of u of internal points is observed to be higher than for the first ($t = 0$) point, if $|\Delta u_{\max} - \Delta u_{\min}| < |u_{\max} - u_{\min}|$.

The decoded and adaptively mapped, discretized values of u are curve-fitted piece-wise (splines) to obtain a continuous function, $u^{(i)}(t)$. A piece-wise cubic Hermite subroutine is used to do this. This continuous function is again digitized to give $N_{\text{sim}} (\geq N_{\text{ga}})$ values of the control variable, $[U^{(i)}(j); j = 1, 2, \dots, N_{\text{sim}}]$. The generation of several additional, intermediate, discretized values of $u^{(i)}$ is necessary for integrating the model differential equations (Eq. 1 and Tables B1-B3).

The digitized temperature history, $[U^{(i)}(j); j = 1, 2, \dots, N_{\text{sim}}]$, corresponding to the i^{th} member of the population, is used in a Gear subroutine³³ (D02EJF in the NAG library) to integrate the balance equations, starting with the initial conditions in Eq. 8 and continuing till $t = t_{\text{fo}}$. The program stores the values of each of the state variables, $\mathbf{x}^{(i)}(j)$, at every intermediate value of t , such that there are N_{sim} sets of \mathbf{x} . The value of $I^{(i)}$ at each of these storage locations is computed, and the location, $t_{\min}^{(i)}$, of the minimum of $I^{(i)}$ as well as the minimum value itself, $I_{\min}^{(i)}$, are obtained by search. Evidently, t_{fo} should be chosen large enough so that I_{\min} occurs in $0 \leq t \leq t_{\text{fo}}$ for all i . The integration of the balance equations and the location of $I_{\min}^{(i)}$ for each of the N_p chromosomes is carried out.

One additional point needs to be emphasized. The computer code, SGA²⁵, which has been used in this study after modification *maximizes* a 'fitness' function, $F^{(i)}$, rather than *minimizes* an objective function, I . Hence, we define a fitness function

$$F^{(i)} \equiv 1 / (1 + I_{\min}^{(i)}) \quad (11)$$

and maximize its value (wherever $I^{(i)}$ is to be minimized).

The next step in GA is to have 'reproduction' in the population of chromosomes. A mating pool is first formed. In this pool, priority is given to those chromosomes which have higher fitness values. The essential idea is to pick out the above-average strings in the current population and include (multiple) copies of these in the mating pool in a probabilistic manner. It is here that the principle of natural selection (survival of the fittest) comes in action. The principle of proportionate reproduction is used. The probability of selecting the i^{th} chromosome in the mating pool is $F^{(i)} / \sum_{i=1}^{N_p} F^{(i)}$. A 'roulette-wheel' (whose circumference is marked for each chromosome proportionate to its fitness value) is spun N_p times. In each spin, the chromosome corresponding to the location of the roulette-wheel pointer is copied into the pool. This thought experiment is implemented using N_p random numbers^{24,25}.

After the mating pool is created, crossover and mutations take place to produce the new population (next generation). These operations take place at the chromosome

(binary) level. Two chromosomes are selected randomly from the mating pool, a crossing site is selected (randomly again), and portions of the chromosomes before and after the crossing site are exchanged. For example, for seven-bit chromosomes with crossing site after the third binary, the crossover is described by:

$$\begin{array}{ccc}
 100|1111 & \longrightarrow & 100\ 0100 \\
 110|0100 & & 110\ 1111 \\
 \text{(old generation)} & & \text{(new generation)} \quad (12)
 \end{array}$$

While performing crossovers, only $N_p p_c$ chromosomes are crossed, the remaining being left untouched (p_c is referred to as the crossover probability).

Another operation, called mutation, is also used to improve the next generation. The mutation operator changes a binary number from 1 to 0 or vice versa, with a probability, p_m . This operation is carried out for each of the $N_p N_{chr}$ bits in the population, again using appropriate random numbers^{24,25}. The need for mutation leads to a local search around the current solution, and helps maintain the diversity of the population²⁵.

The random crossover procedure discussed above leads to a preponderance of crossovers in the (inactive) range, $t_{min}^{(i)} \leq t \leq t_{fo}$, if the guess value of t_{fo} supplied to the computer code is too large. This procedure, thus, needs to be adapted so that crossovers take place in a t -domain (horizon) which becomes smaller over generations. What is done is to limit crossovers to

$0 \leq t \leq t_{\min, \text{best}} \times (1 + S)$, where $t_{\min, \text{best}}$ is the best (minimum) of the N_p values of $t_{\min}^{(i)}$ in any generation, and S is a safety factor supplied to the program (obtained by numerical experimentation). The string length corresponding to $t_{\min, \text{best}}(1 + S)$ is given by

$$N'_{\text{chr}} = N_{\text{chr}} t_{\min, \text{best}}(1 + S) / t_{\text{fo}} \quad (13)$$

where N'_{chr} is an (next higher) integer. The region in which crossovers take place would decrease from generation to generation as $t_{\min, \text{best}}$ decreases. Such an adaptation of the conventional GA can be used to advantage for any minimum time optimization problem, and provides an automatically narrowing crossover horizon.

The optimal solutions generated using GA can be compared with those obtained (for the same objective function, constraints and model equations) from Pontryagin's minimum principle²⁷⁻³⁰ using the first order control vector iteration technique (referred to as P1). The algorithm to be used is summarized in Table 3, and is an adaptation of that used by Vaid and Gupta³⁴ and Ray and Gupta³⁵ earlier.

TABLE 3

FORMULATION OF THE OPTIMAL CONTROL PROBLEM USING
PONTYAGIN'S MINIMUM PRINCIPLE²⁷⁻³⁰ WITH FIRST ORDER
CONTROL VECTOR ITERATION METHOD

Optimization problem

$$\text{Max } I [\underline{u}(t)] = G [\underline{x}(t_f)]$$

s.t.

$$\frac{d\underline{x}}{dt} = \underline{F}(\underline{x}, \underline{u})$$

$$\underline{u}_{\min} \leq \underline{u}(t) \leq \underline{u}_{\max}$$

Here,

$$G [\underline{x}(t_f)] = - [t_f + w_1 (1 - x_{mf}/x_{md})^2 + w_2 (1 - \mu_{nf}/\mu_{nd})^2]$$

Procedure

- 1) Guess $\underline{u}(t) = T^{(0)}(t)$; $0 \leq t \leq t_{f0}$
- 2) With this $\underline{u}(t)$, integrate the state variable equations
 $\frac{d\underline{x}}{dt} = \underline{F}(\underline{x}, \underline{u})$ to obtain $\underline{x}(t)$; $0 \leq t \leq t_f$,
with t_f obtained by solving

$$H(t_f) = (\partial G / \partial \underline{x}) \underline{F} |_{t=t_f} = 0$$

- 3) With the values of $\underline{x}(t)$ and $\underline{u}(t)$, integrate the
adjoint equations backwards from $t = t_f$ to $t = 0$,

$$\frac{d\lambda^T}{dt} = - (\partial H / \partial \underline{x}) ; \quad \lambda^T(t_f) = \partial G / \partial \underline{x} |_{t=t_f}$$

$$\text{where } H \equiv \lambda^T \underline{F}$$

- 4) Correct $\underline{u}(t)$ by,

$$\underline{u}(t) = \underline{u}(t) + \epsilon (\partial H / \partial \underline{u}), \quad \epsilon > 0$$

- 5) Perform a single variable search (on ϵ) to
generate several $\underline{u}(t)$, obtain I for each of these
histories (after integrating the state variable equations
for each case), then obtain ϵ_{opt} corresponding to

Contd...3b

Table 3 (contd...b)

the maximum value of I (note that $\partial H/\partial u$ is not updated during this search).

6) Update $u(t)$ by,

$$u^{\text{new}}(t) = u^{\text{old}}(t) + \varepsilon_{\text{opt}} (\partial H/\partial u)$$

and return to step 2.

7) Iterate until convergence is attained.

CHAPTER 3

RESULTS AND DISCUSSION

Several checks were made to ensure that the computer code prepared was free of errors. The code was used to generate the monomer conversion and the number average chain length for different isothermal conditions. These were found to match the results of Seth and Gupta¹⁹ and are shown in Fig. 2 for an initial initiator concentration, $[I]_0$, of 25.8 mol/m^3 (reference value). These results were generated with a value of TOL of 10^{-7} in the code DO2EJF, and no significant differences were found upon decreasing the value of this parameter. This check indicated that the simulation part of our code was free of errors, and also provided results which could be used to explain optimal histories qualitatively. The next check was on the correctness of the optimization part of our program. From Fig. 2, it is clear that if we use

$$\begin{aligned}x_{md} &= 0.0134 \\ \mu_{nd} &= 2365 \\ 60^\circ\text{C} &\leq T(t) \leq 90^\circ\text{C}\end{aligned}\tag{14}$$

the optimal temperature history would be isothermal at 60°C (any higher temperature would give lower values of μ_{nf} while simultaneously giving higher x_{mf}). Also, under these isothermal conditions, the value of t_f would be 230.77 s. Similarly, for

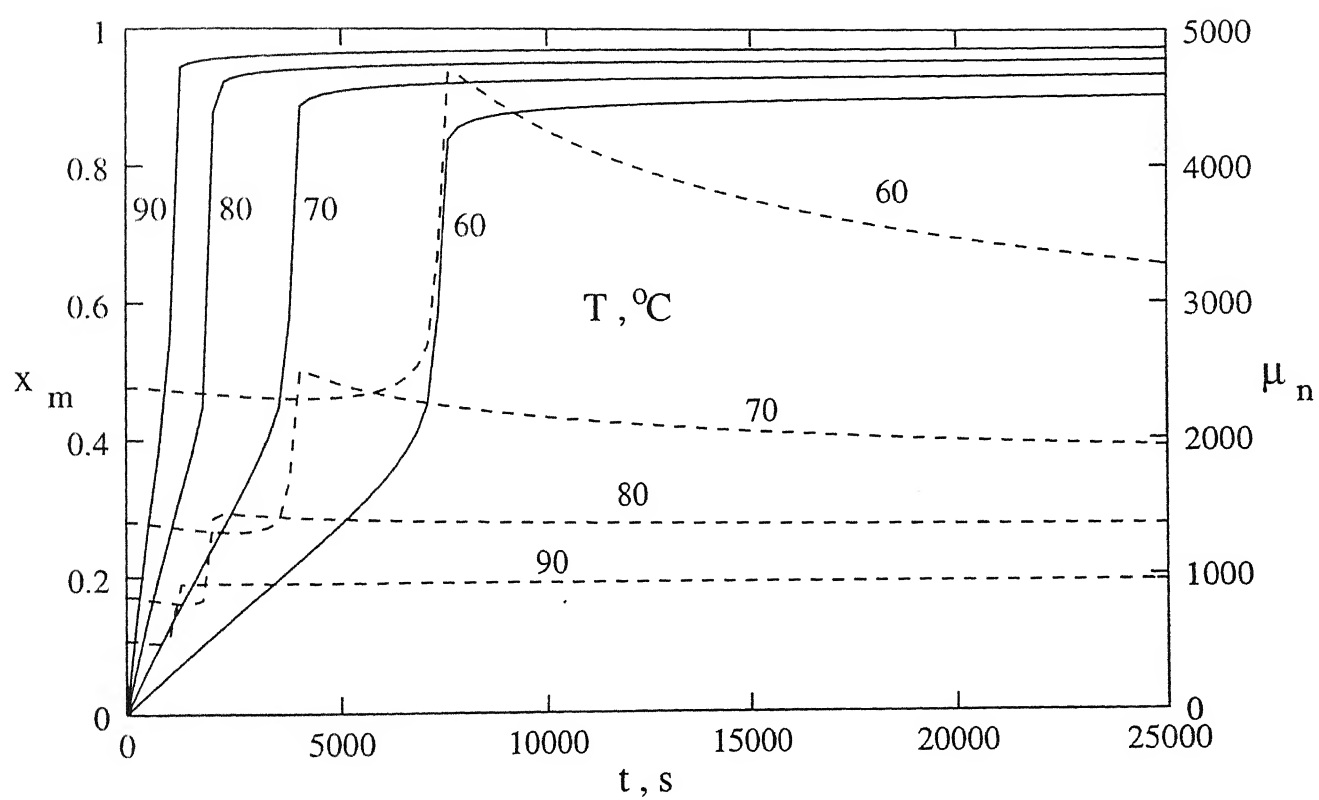


Fig. 2 : $x_m(t)$ (solid) $\mu_n(t)$ (dotted) for isothermal bulk polymerization of MMA using AIBN ($[I]_0 = 25.8 \text{ mol m}^{-3}$)

$$\begin{aligned}
x_{md} &= 0.4926 \\
\mu_{nd} &= 532.16 \\
60^{\circ}\text{C} &\leq T(t) \leq 90^{\circ}\text{C}
\end{aligned} \tag{15}$$

the optimal $T(t)$ would be isothermal at 90°C (see Fig. 2), with $t_f = 969.67$ s (any lower temperature would lead to higher values of μ_{nf} , while simultaneously leading to lower x_{mf}). The optimization problems described in Eqs. 14 and 15 were solved using the GA computer code (using the parameters of Table 4) and in both cases, the expected optimal temperature histories were obtained (in 8 generations for Eq. 14 and 3 generations for Eq. 15, shown in Figs. A1-A2 in Appendix A). A similar check was made for the computer code using Pontryagin's principle with the first order control vector iteration method (P1). The starting guess for this technique was $T^{(0)} = 90^{\circ}\text{C}$ (for Eq. 14) and $T^{(0)} = 60^{\circ}\text{C}$ (for Eq. 15). Again, the expected isothermal optimal histories were obtained (Figs. A1-A2 in Appendix A) in 2 and 8 iterations (for Eqs. 14 and 15, respectively). These checks gave confidence on both our computer codes, GA and P1.

The optimization program using GA was now run for

$$\begin{aligned}
x_{md} &= 0.94 \\
\mu_{nd} &= 1800
\end{aligned} \tag{16}$$

These values are quite close to those used by Vaid and Gupta,³⁴ as well as other workers, and are being used as reference values to illustrate the working of GA. Fig. 3 shows how the optimal temperature history (the best for each generation) evolves over

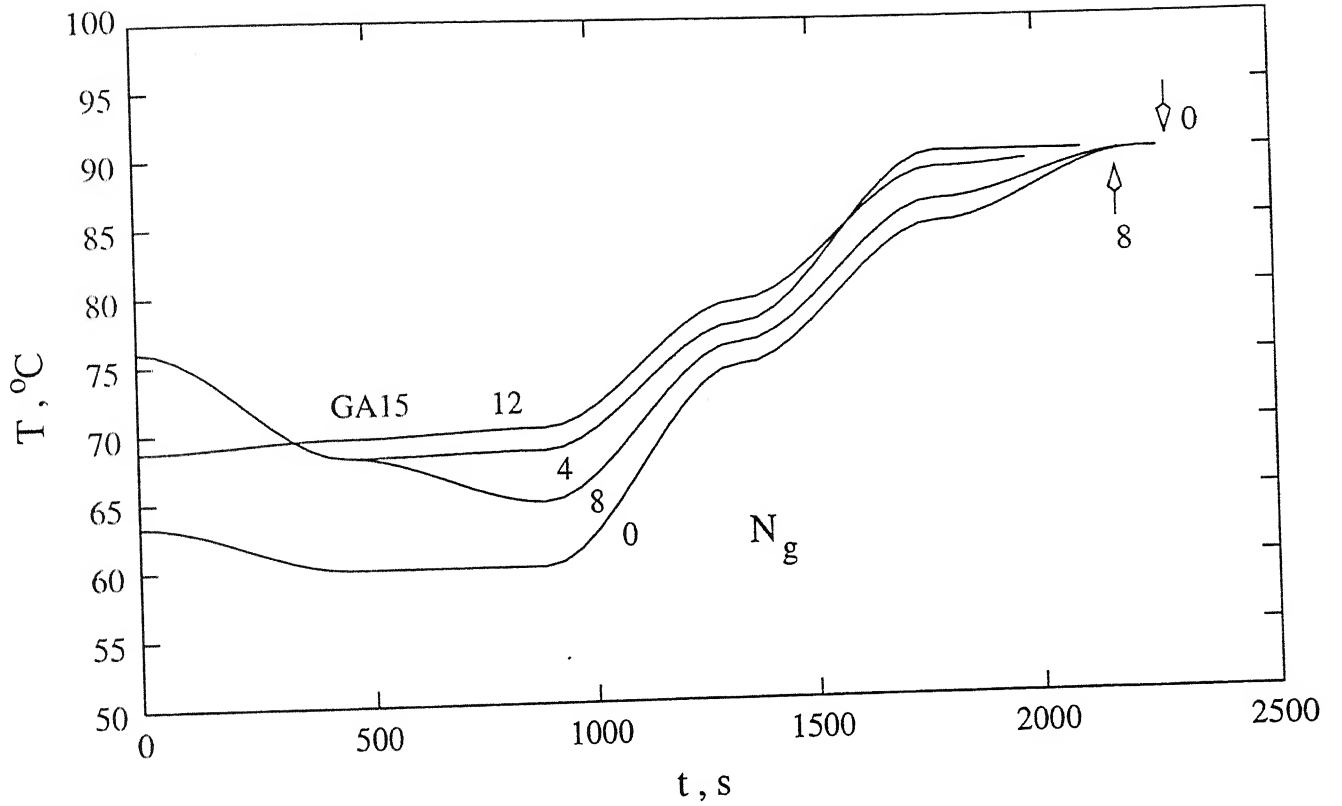


Fig. 3 : Evolution of temperature histories towards the optimal one , with generation number , N_g , corresponding to $x_{md} = 0.94$, $\mu_{nd} = 1800$ (for parameters of Table 5) . Arrows indicate the end points of corresponding curves .

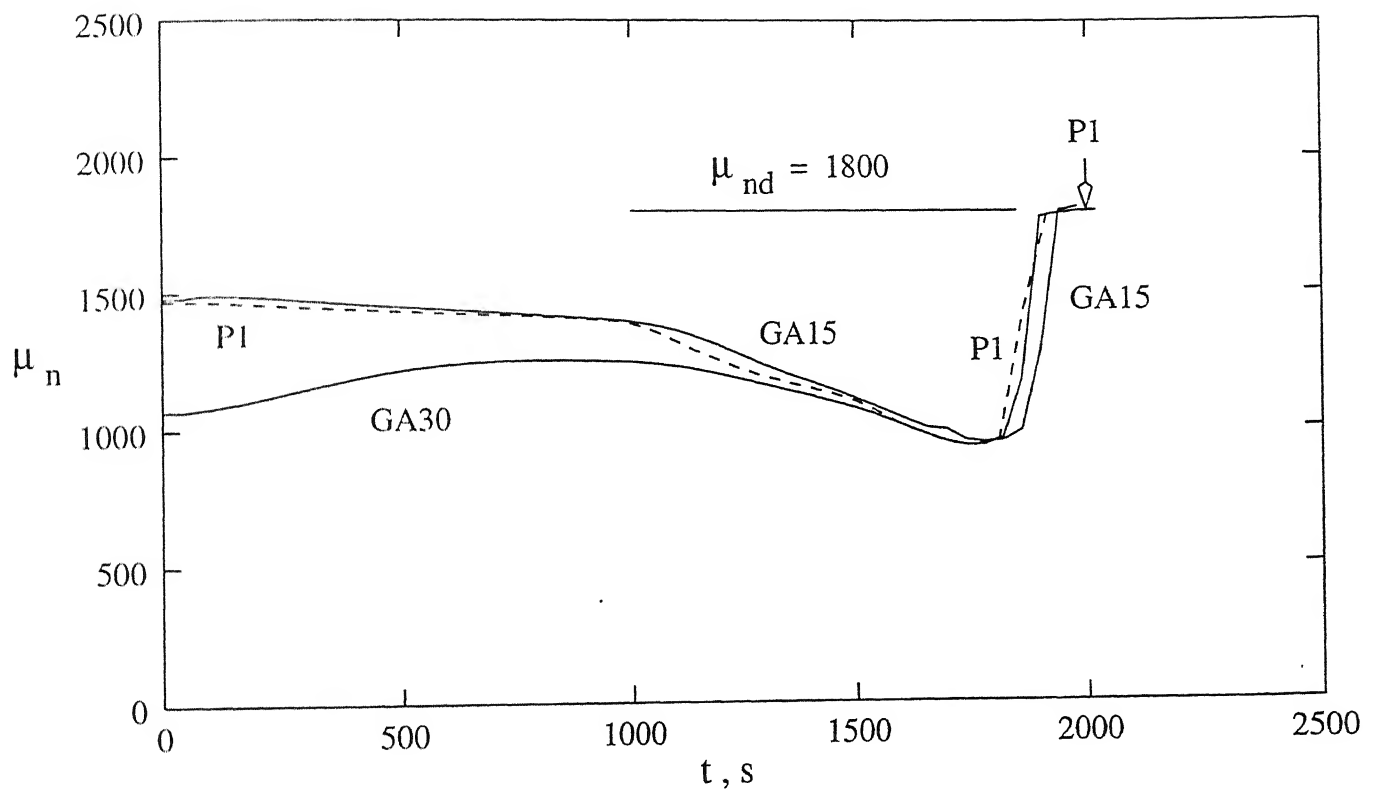


Fig. 4 : $\mu_n(t)$ corresponding to $T_{opt}(t)$ for the GA15 run , as well as for those corresponding to Fig. 6 .

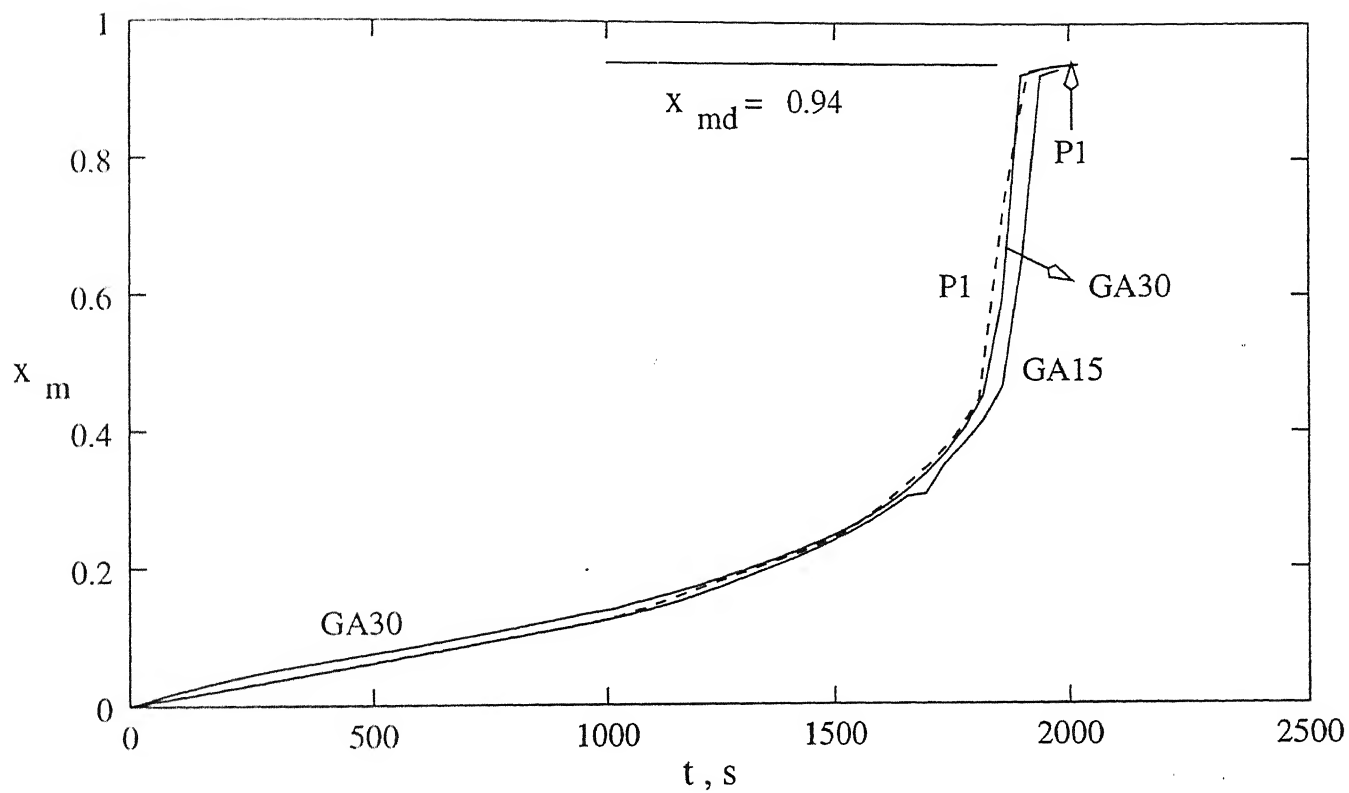


Fig. 5 : $x_m(t)$ corresponding to $T_{opt}(t)$ for the GA15 run , as well as
for those corresponding to Fig. 6 .

TABLE 4

PARAMETERS USED FOR REFERENCE RUN

GA Parameters

$$N_p = 100$$

$$N_{str} = 7$$

$$N_{ga} = 10$$

$$N_{sim} = 100$$

$$[u_{min}, u_{max}] = [60, 90] ; ^\circ C$$

$$[\Delta u_{min}, \Delta u_{max}] = [-15, +15] ; ^\circ C$$

$$p_c = 0.99$$

$$p_m = 0.000009$$

$$S = 0.2$$

$$t_{fo} = 4000 \text{ s}$$

$$w_1 = w_2 = 2.5 \times 10^5$$

In addition, the value of the parameter, RS, used²⁵ for generating binaries is 0.9.

Design Parameters

$$x_{md} = 0.94$$

$$\mu_{nd} = 1800$$

$$[I]_0 = 25.8 \text{ mol/m}^3$$

generations. Very little improvement takes place after about 12 generations and so, results for $N_g > 12$ are not shown. The CPU time for generating these results was 15.8 s on a DEC 3000 α xp. The variation of μ_n and x_m with time, using the optimal temperature history (for $N_g = 12$) shown as GA15 (15 indicating Δu_{\min} and Δu_{\max} of -15 and $+15^\circ\text{C}$) in Fig. 3, are shown in Figs. 4 and 5 (by solid lines marked GA15). Some amount of oscillations are observed in the optimal temperature history (Fig. 3), which could be reduced by changing some of the parameters in Table 4 (see later). Fig. 6 compares the optimal history (curve GA15; same as for $N_g = 12$ in Fig. 3) with that obtained using Pontryagin's minimum principle (curve P1, obtained by starting with $T^{(0)} = 90^\circ\text{C}$ and converging in about 8 iterations). The values of the objective function, I , for the GA15 and the P1 cases are found to be 2008.36 and 2016.96, respectively. The two histories are also observed to be fairly close to each other. It may be noted^{24,25,27-30} that both GA and P1 lead to near-optimal solutions only and become very sluggish as the optimal history is approached. The agreement in Fig. 6 is, thus, extremely good (perhaps fortuitously so). It is interesting to observe from Figs. 3 and 4 that optimal operation requires relatively low temperatures [leading to relatively high values of μ_n (see Fig. 4)], followed by a gradual increase in $T(t)$ [associated with some fall in μ_n] to its maximum value of 90°C . The value of μ_n builds up to its desired value by exploiting the gel effect near the end, this being exhibited as a

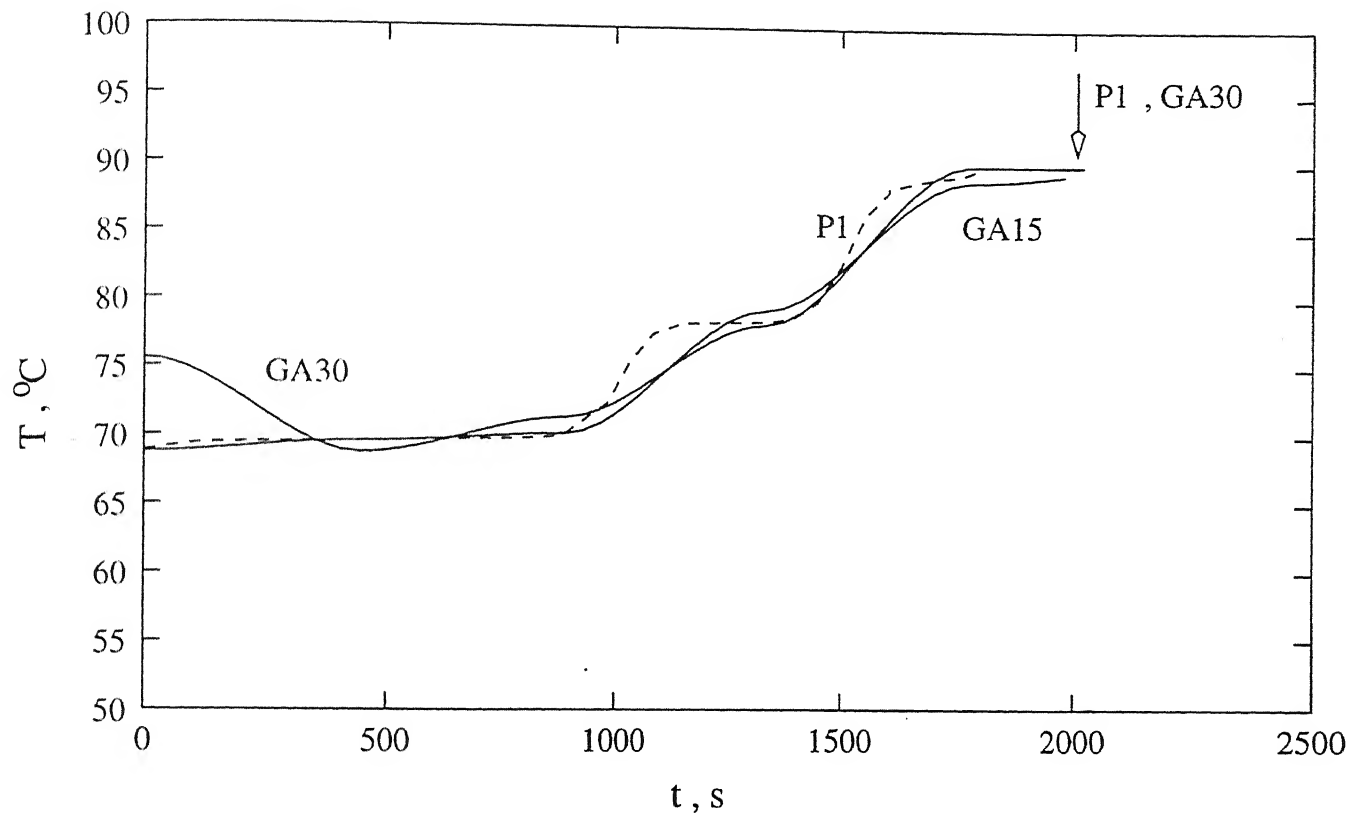


Fig. 6 : $T_{opt}(t)$ corresponding to the conditions of Fig. 3 using the P1 (dotted) and GA (solid) techniques. GA15 corresponds to the reference run (Table 5) while GA30 corresponds to $[\Delta T_{min}, \Delta T_{max}] = \pm 30^{\circ}\text{C}$ (all other parameters same as given in Table 5). Arrow indicates t_f for P1.

sharp increase in $\mu_n(t)$ and $x_m(t)$ near $t \approx t_f$. The sudden increase in $\mu_n(t)$ to its final value of μ_{nd} is a characteristic of almost all optimal solutions obtained in our study, and emphasizes the need for model-based on-line optimizing control in the period prior to the onset of the gel effect.

Computations were carried out using Pontryagin's minimum principle (first order) for the conditions described in Eq. 16, but using the initial guess, $T^{(o)}(t)$, different than that used for generating Figs. 4-6 [i.e., isothermal $T^{(o)}(t)$ different from 90°C , see Figs. A3-A5 in Appendix A]. It was found that the (sub-) optimal temperature histories were very sensitive to the initial guess, and that there was only a very narrow window of the initial guess for which converged solutions were obtained which were similar to GA15. A similar acute sensitivity to the initial guess history was also observed by Vaid and Gupta³⁴ who used a similar algorithm but solved a slightly different optimization problem. In fact, we obtained different (sub-) optimal temperature histories on using different $T^{(o)}(t)$ outside of the narrow window. In each case, the x_{mf} and μ_{nf} were very close to their desired values, while the values of I differed *slightly*. This could be because of two possible reasons. Firstly, the value of I_{opt} is *relatively* insensitive to $T_{opt}(t)$, and secondly, there could be several shallow, *local* minima, and P1 converges to (near) these, depending on the initial guess, $T^{(o)}(t)$, provided. Which of these two causes leads to the ineffectiveness of the P1 technique is not clear, nor

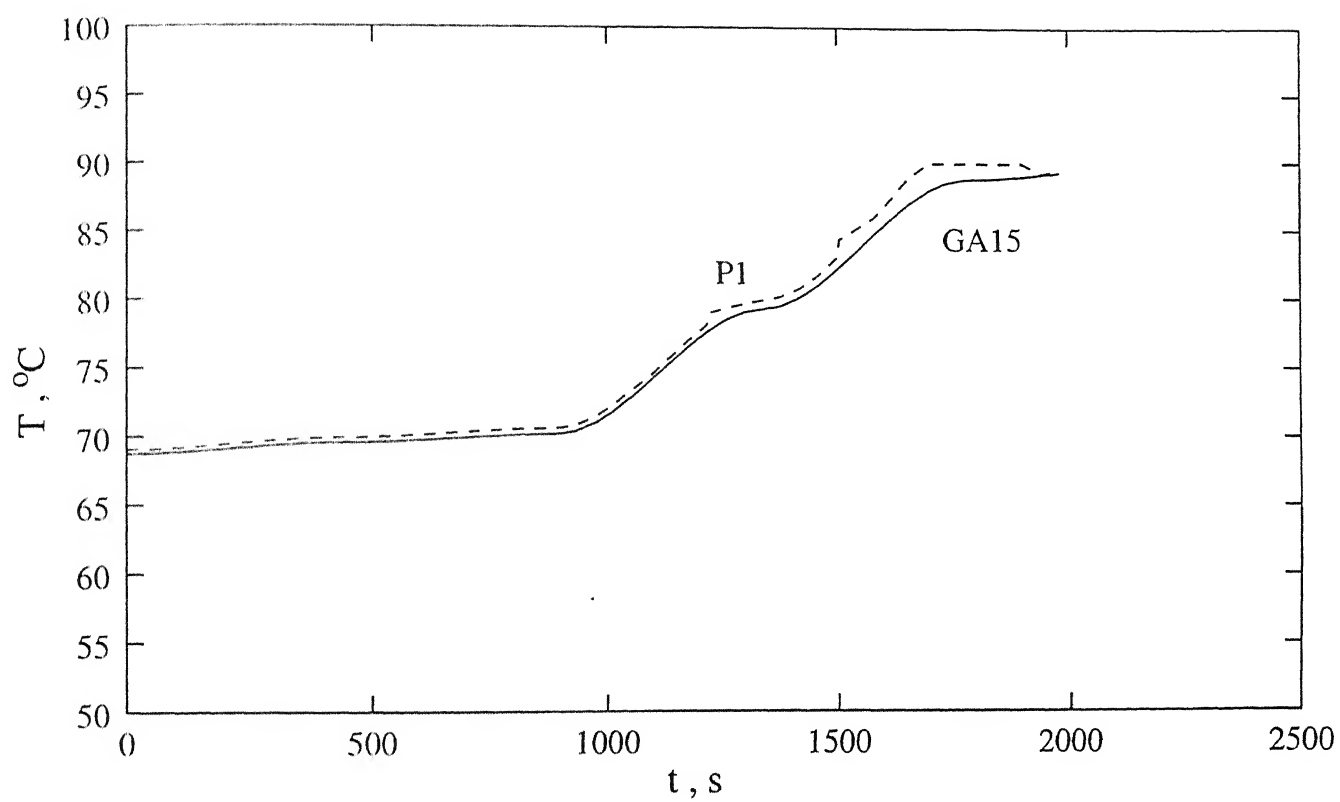


Fig. 7 : $T_{\text{opt}}(t)$ obtained with the P1 (dotted) technique using the optimal history from GA15 (solid) as an initial guess.

is this answer too important. However, GA is known^{24,25} to reach the *global* optimum, and is robust, and so we believe that its solution is the 'true' one. The P1 technique *also* converges to the solution provided by GA if we start from $T^{(0)} = 90^{\circ}\text{C}$, or use $T^{(0)}(t)$ somewhat similar (but not identical) to the optimal history provided by GA.

This drawback of the P1 technique can be overcome by the use of GA to first generate near-optimal solutions which can be provided as initial guesses, to be improved upon by using P1. We believe that GA followed by P1 is a superior combination than the first order Pontryagin technique followed by the second order (P2) technique²⁷⁻³⁰, in which second order derivatives are required. Fig. 7 shows the improvement of the optimal $T(t)$ using the GA15-P1 combination. The value of I of 2008.71 corresponding to GA15 is reduced to 1980.34 using the P1 technique. Similar improvements in the value of I have been found in other cases of GA + P1 tried in this study (detailed results can be provided on request).

We now study the effect of varying the parameters (Table 4) used in GA. Details of the parameters which are varied *one at a time*, keeping all others at their reference values (Table 4), are given in Table 5. Fig. 8 shows that in the initial region (low t), the optimal temperature history is somewhat sensitive to the number, N_p , of chromosomes in the population (curves 1 and 2). However, changing N_p could lead to oscillatory behavior in $T_{\text{opt}}(t)$, which needs to be dampened by changing some *other*

TABLE 5
SOME DETAILS CORRESPONDING TO $T_{opt}(t)$ SHOWN IN FIGS. 8-14

| Curve No. | Parameter Varied | Parameter Value (Ref.value) | I_{opt} | * N_g | Fig.No. |
|-----------|--------------------------------------|--|-----------|---------|---------|
| GA15 | --- | Table 4 | 2008.36 | 12 | 8 |
| 1 | N_p | 50 (100) | 2076.49 | 9 | 8 |
| 2 | N_p | 200 (100) | 1953.89 | 15 | 8 |
| 3 | N_{str} | 14 (7) | 1959.63 | 18 | 8 |
| 4 | N_{ga} | 20 (10) | 2065.29 | 13 | 9 |
| 5 | N_{ga} | 30 (10) | 2191.00 | 10 | 9 |
| 6 | P_m | 10^{-5} (9×10^{-6}) | 2265.56 | 14 | 10 |
| 7 | P_c | 0.98 (0.99) | 2101.24 | 14 | 10 |
| 8 | N_{sim} | 80 (100) | 2128.62 | 16 | 10 |
| 9 | RS | 0.6 (0.9) | 1946.64 | 17 | 10 |
| 10 | ΔT_{min} ΔT_{max} | $\pm 20^{\circ}C$ ($\pm 15^{\circ}C$) | 2021.63 | 7 | 11 |
| 11 | ΔT_{min} ΔT_{max} | $\pm 30^{\circ}C$ ($\pm 15^{\circ}C$) | 2020.52 | 7 | 11 |
| 12 | S | 0.4 (0.2) | 2141.61 | 10 | 11 |
| 13 | x_{md} | 0.95 (0.94) | 2384.44 | 16 | 12 |
| 14 | μ_{nd} | 1600 (1800) | 1850.98 | 17 | 13 |
| 15 | μ_{nd} | 2000 (1800) | 2294.14 | 17 | 13 |
| 16 | $[I]_O$ | 15.48 (25.8) | 1629.82 | 6 | 13 |

* For achieving convergence

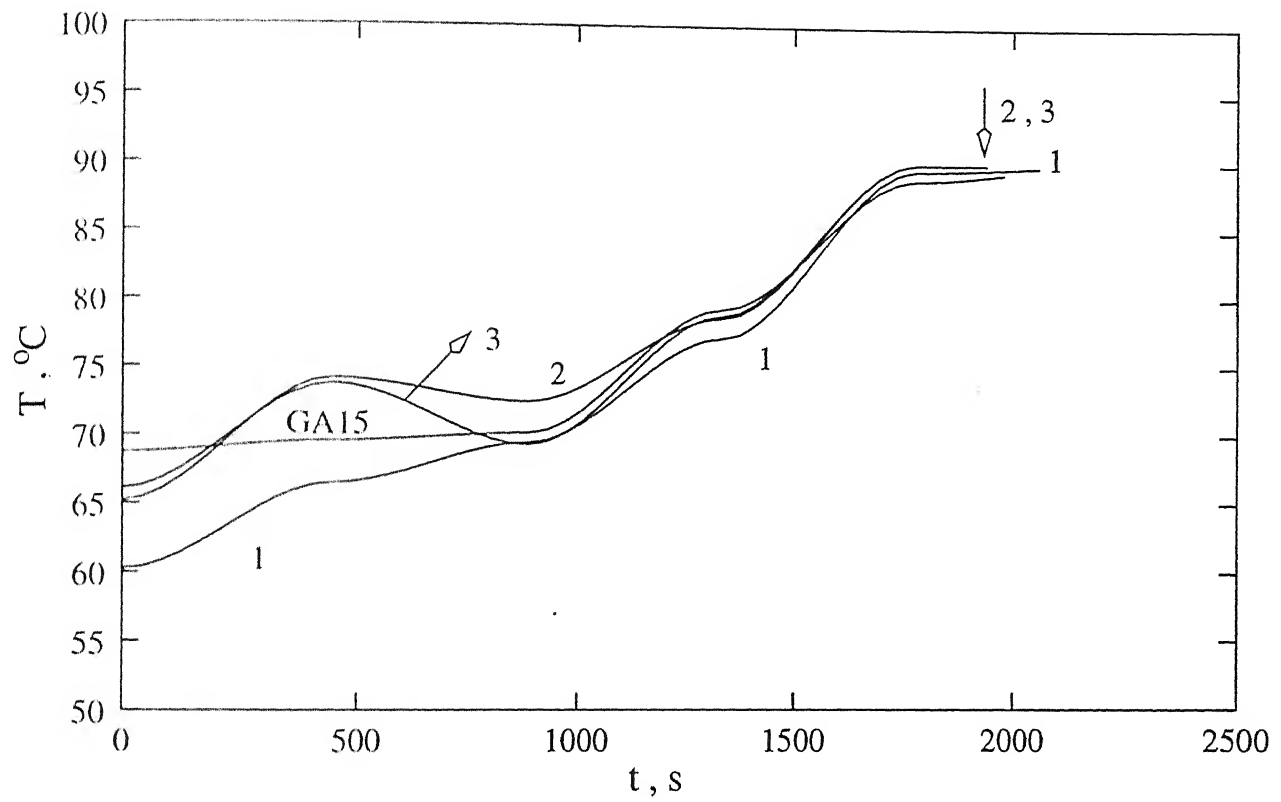


Fig. 8 : Effect of varying N_p and N_{str} on the optimal temperature histories . Curve 1 : $N_p = 50$; curve 2 : $N_p = 200$; curve 3 : $N_{str} = 14$. Results for the reference run (GA15) also shown for comparison .

parameter (e.g., Δu_{\min} , Δu_{\max}) *simultaneously*. In fact, the reference values of the parameters (run GA15) have been chosen such that the oscillations are minimized for this run. Similar oscillatory behavior is observed (curve 3, Fig. 8) in the initial region by increasing N_{str} from 7 (ref) to 14. It is clear that any change made to improve the accuracy of results leads to more oscillations in the initial region, and its effects need to be dampened out. A similar conclusion is obtained on studying curves 4 and 5 in Fig. 9 and curve 8 in Fig. 10. As N_{ga} is increased, $T_{\text{opt}}(t)$ oscillates considerably, to the extent that I_{opt} worsens. The effect of increasing the mutation probability is similar. Decreasing the crossover probability from 0.99 to 0.98 (curve 7, Fig. 10) does not lead to oscillations, but worsens I_{opt} slightly. The effects of decreasing N_{sim} and changing RS are also shown (curves 8 and 9) in Fig. 10.

Fig. 11 shows the effect of varying the parameter characterizing one of the adaptations of the conventional GA, namely, use of Δu_{\min} and Δu_{\max} as constraints. These were introduced to dampen oscillations in $T_{\text{opt}}(t)$, as well as to ensure implementability of the optimal history in industrial systems. The actual values of ΔT_{\min} and ΔT_{\max} to be used should really be decided by the heat transfer limitations of the reactor, but these have been considered as parameters and chosen somewhat arbitrarily here to study their effect. It is observed that increasing the range of ΔT from ± 15 to ± 30 $^{\circ}\text{C}$ leads, as expected, to more

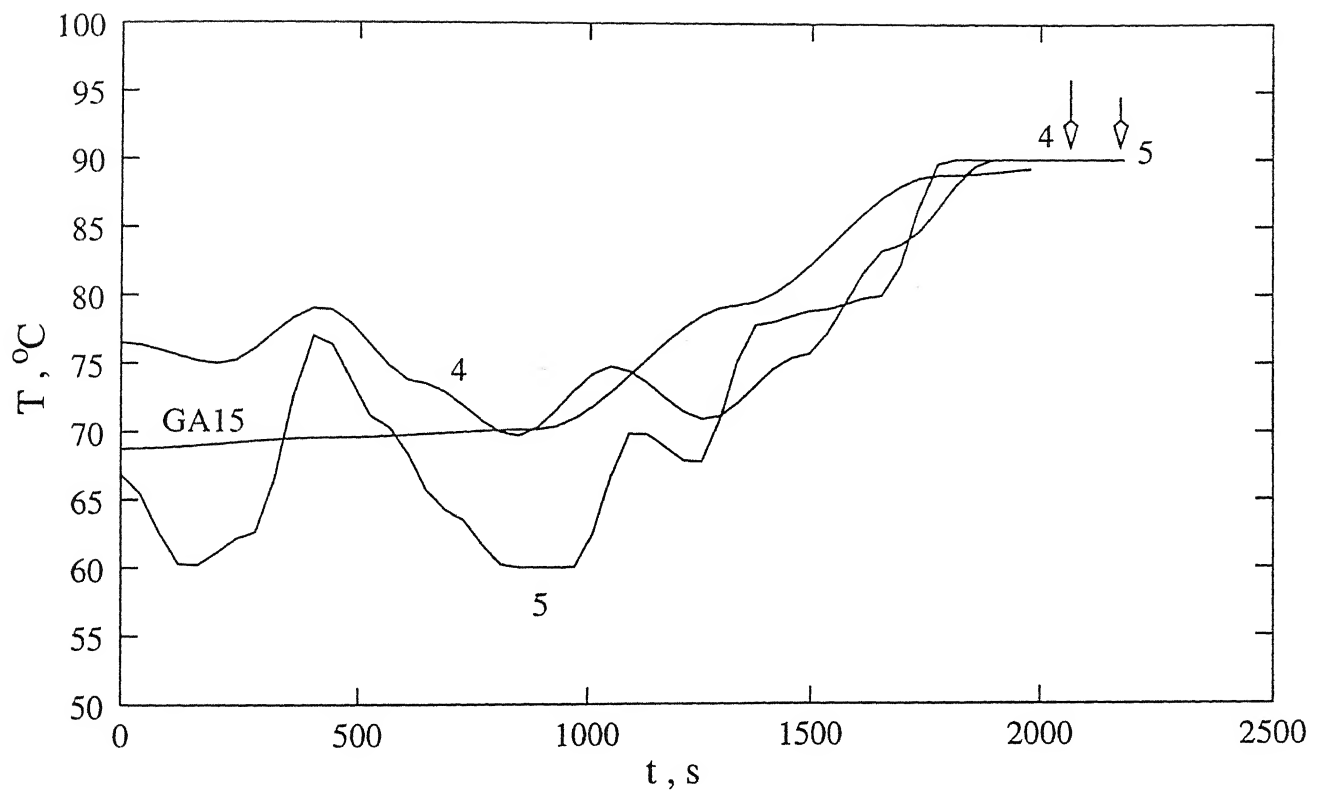


Fig. 9 : Effect of varying N_{ga} on the optimal temperature history . Curve 4: $N_{ga} = 20$;
 curve 5 : $N_{ga} = 30$.

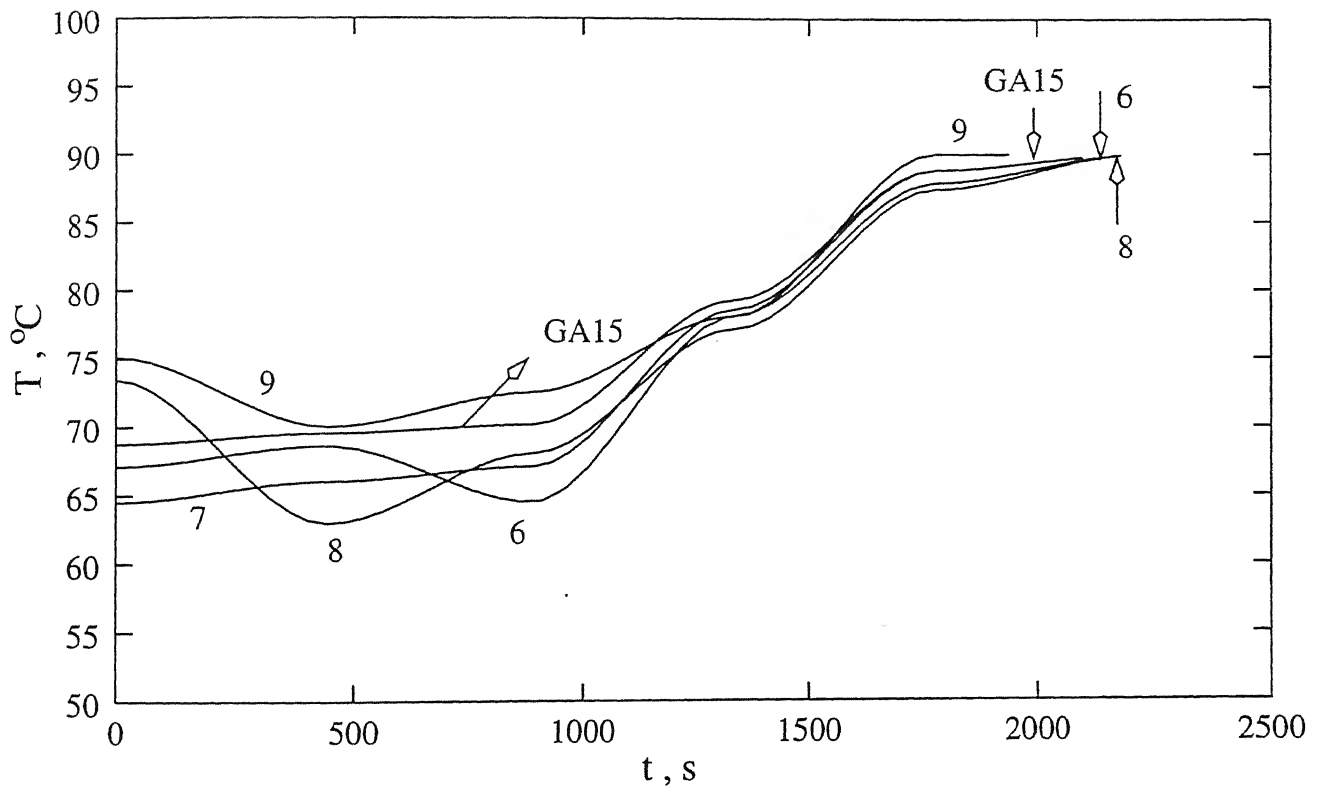


Fig. 10 : Effect of varying p_m , p_c , N_{sim} and RS on the optimal temperature history .

Curve 6 : $p_m = 10^{-5}$; $p_c = 0.98$; curve 8 : $N_{sim} = 80$.

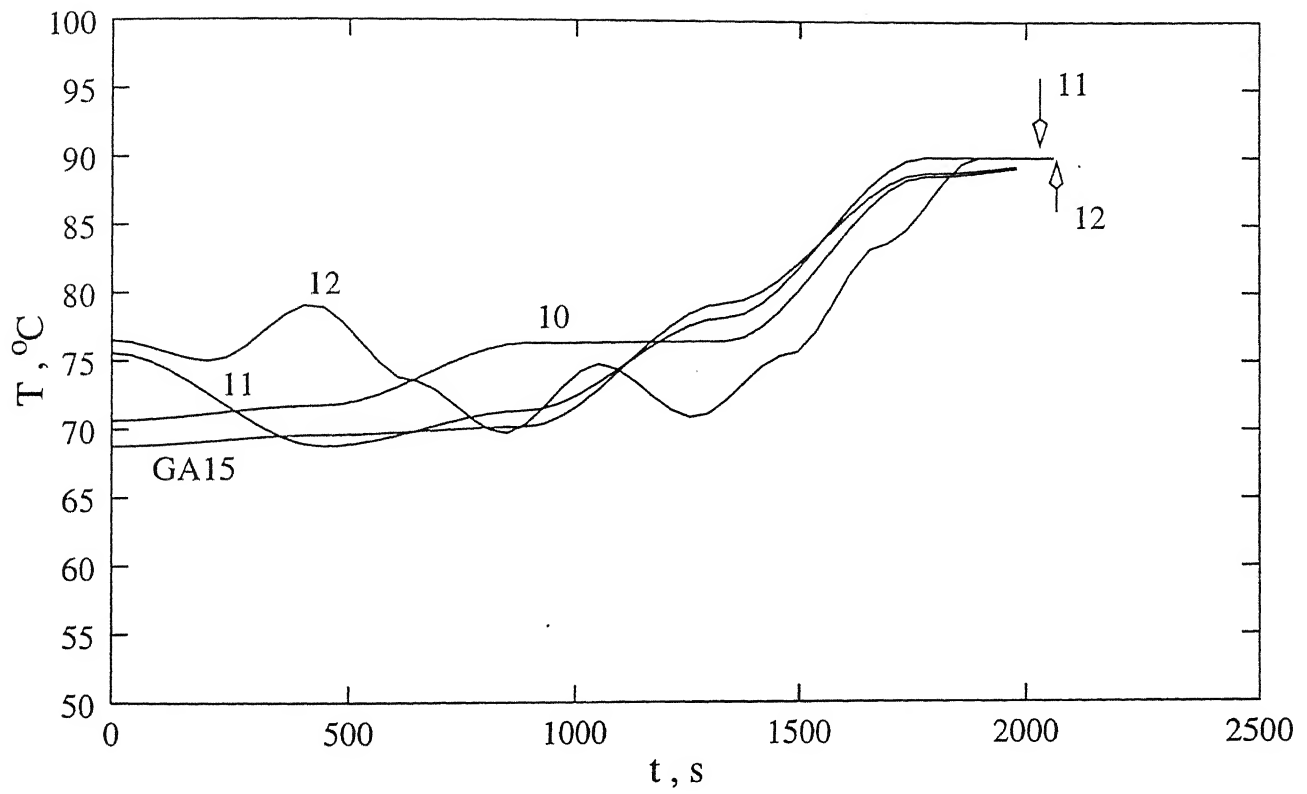


Fig. 11 : Effect of varying $[\Delta T_{\min}, \Delta T_{\max}]$ and S on the optimal temperature history .
 Curves 10 and 11 : $[\Delta T_{\min}, \Delta T_{\max}] = \pm 20^{\circ}\text{C}$ and $\pm 30^{\circ}\text{C}$, respectively .
 Curve 12 : $S = 0.4$.

oscillations, and to a worsening of I_{opt} . It is interesting to compare curve 11 (for $-30 \leq \Delta T \leq 30^{\circ}\text{C}$, i.e., no constraint is operative on the temperature of a neighboring point, except $60^{\circ}\text{C} \leq T \leq 90^{\circ}\text{C}$) with the results from the P1 technique [with $T^{(o)}(t) = 90^{\circ}\text{C}$] where no constraint on the temperatures of neighbouring points are operative. Fig. 6 shows that curve 11 (renamed GA30) does not compare as well with curve P1 *quantitatively*, as does the GA15 results due to the oscillations present in GA30. Use of a damping mechanism through ΔT_{min} and ΔT_{max} , thus, appears justified.

Fig. 11 also shows (curve 12) the effect of increasing the safety factor, S , a parameter reflecting another adaptation we have made in the conventional GA. Increasing S leads to a larger domain in which crossovers are permitted, and slows down the rate of convergence (note that GA, too, becomes sluggish as the optimal history is attained, and the results in Figs. 8-11 are all near-optimal in that sense).

The general conclusion from this parametric sensitivity study is that we need to experiment with the several parameters to obtain good, sub-optimal u-histories with GA. Since the histories are global (sub-) optimal solutions, we can follow up GA with the first order Pontryagin (P1) technique to get good final results. This combination exploits the best features of both these techniques.

Figs. 12 and 13 show the effect of varying the 'design'

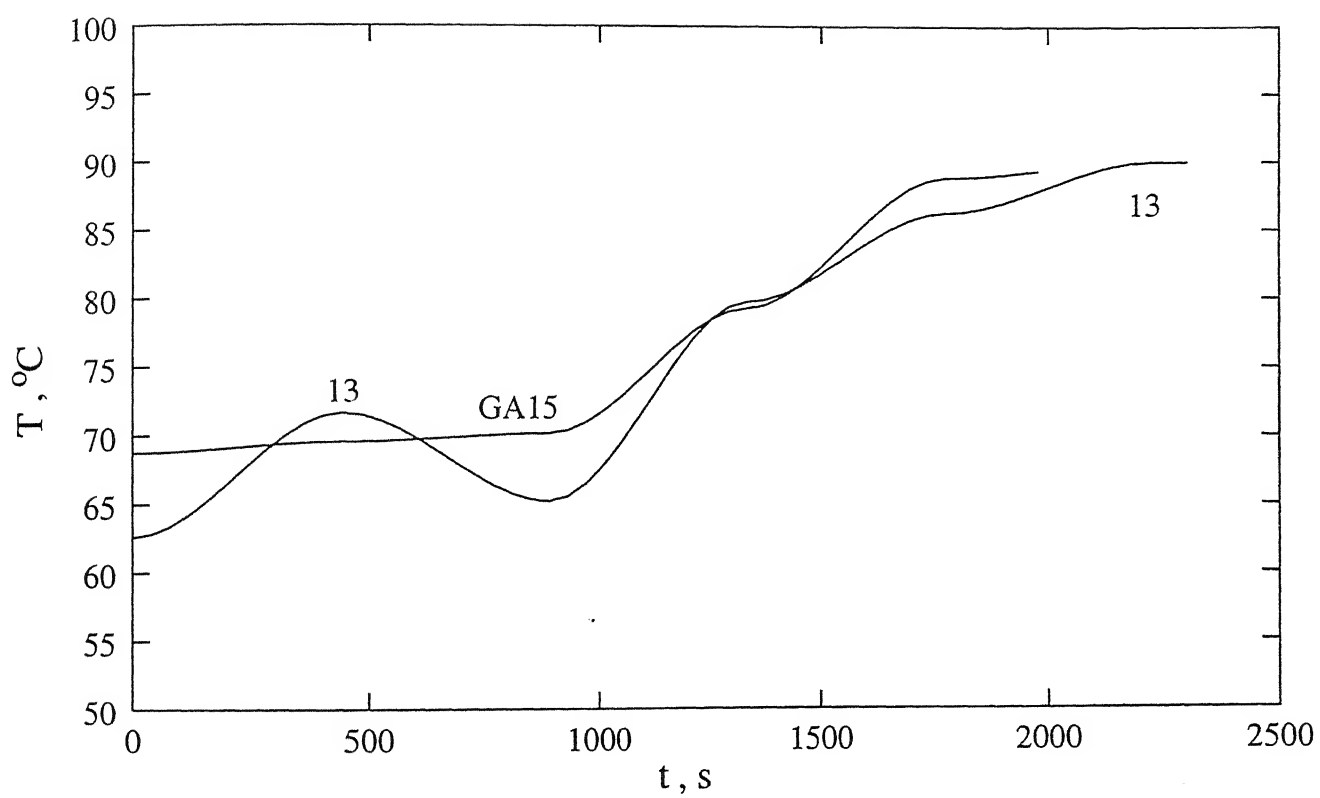


Fig. 12 : Effect of varying x_{md} on the optimal temperature histories . Curve 13 corresponds to $x_{md} = 0.95$.

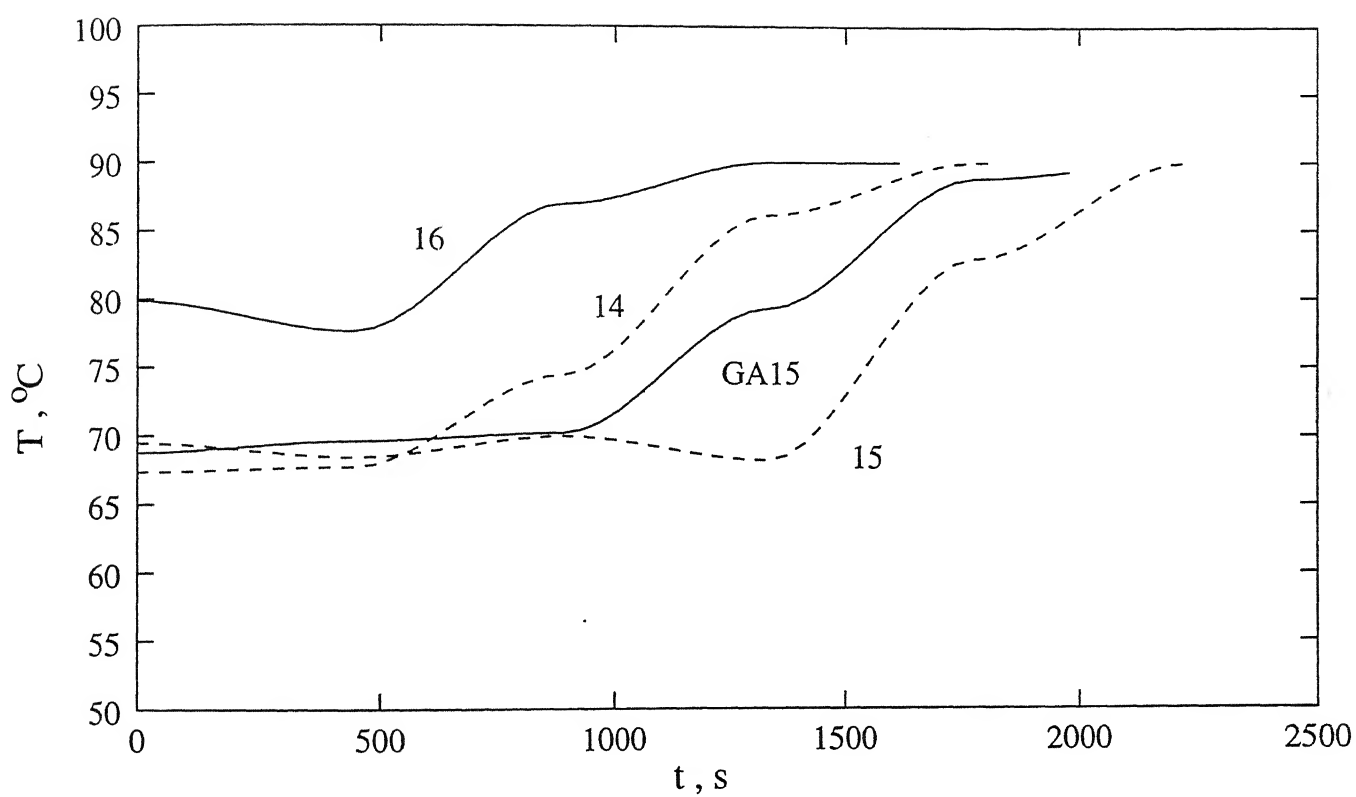


Fig. 13 : Effect of varying μ_{nd} and $[I]_0$ on the optimal temperature histories . Curves 14 and 15 : $\mu_{nd} = 1600$ and 2000 , respectively ; curve 16 : $[I]_0 = 15.48 \text{ mol/m}^3$.

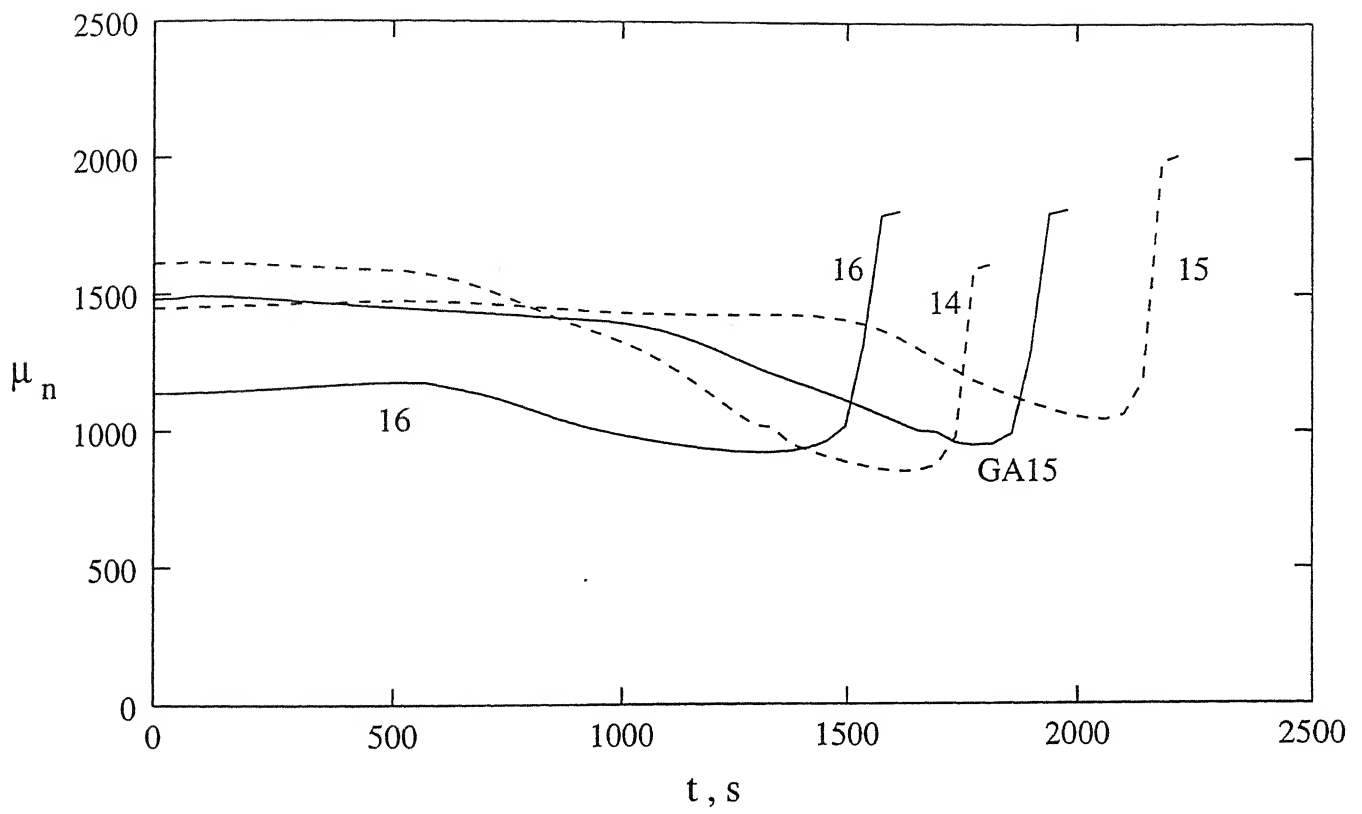


Fig. 14: $\mu_n(t)$ corresponding to the optimal temperature histories given in Fig. 13 .

variables, x_{md} , μ_{nd} and $[I]_0$. Fig. 12 (curve 13) shows that somewhat lower initial temperatures and slower rates of rise of $T(t)$ are required to obtain higher final values of the monomer conversion if we wish to keep μ_{nd} unchanged. The presence of oscillations in $T_{opt}(t)$ indicates that the reference values of the parameters used are not appropriate to generate the results for this case, and need to be 'retuned' if we wish to have better results. Fig. 13 (curves 14 and 15) shows how the increase of $T_{opt}(t)$ should be delayed to give higher μ_{nf} products. Fig. 14 shows the delayed gel effect helping achieve higher μ_{nf} products. The effect of decreasing the initiator loading, $[I]_0$, is also shown in Fig. 13 (curve 16). Higher temperatures are necessary with lower $[I]_0$ to speed up the reaction, so that t_f is minimized.

The general trends observed in all these cases is that optimal temperature histories for MMA polymerization are such that, initially, we have almost constant μ_n . This is followed by a period during which μ_n decreases (as T goes up). Finally, the gel-effect occurs which leads to a relatively rapid increase in x_m and μ_n to their desired values. The temperatures in the pre-gel effect region are quite important, particularly since rapid changes in T after the onset of the gel effect are not easy to implement. This points out the need for using model-based on-line optimizing control. It is difficult to predict the qualitative trends of $T_{opt}(t)$ intuitively using the isothermal results shown in Fig. 2, and this emphasizes the importance of such quantitative

studies.

The variation of the polydispersity index (PDI, see Nomenclature) of the polymer with time, under optimal conditions (GA15), is shown in Fig. 15. The final value of the PDI is observed to be substantially lower than that of polymer produced under isothermal conditions, which is a blessing in disguise, since reduction of the PDI was not envisaged in our optimization problem (Eq.6). There appears to be some controversy in the literature regarding whether the minimum time problem ensures *simultaneously*, minimum PDI³⁴. Our results indicate substantial lowering of the PDI.

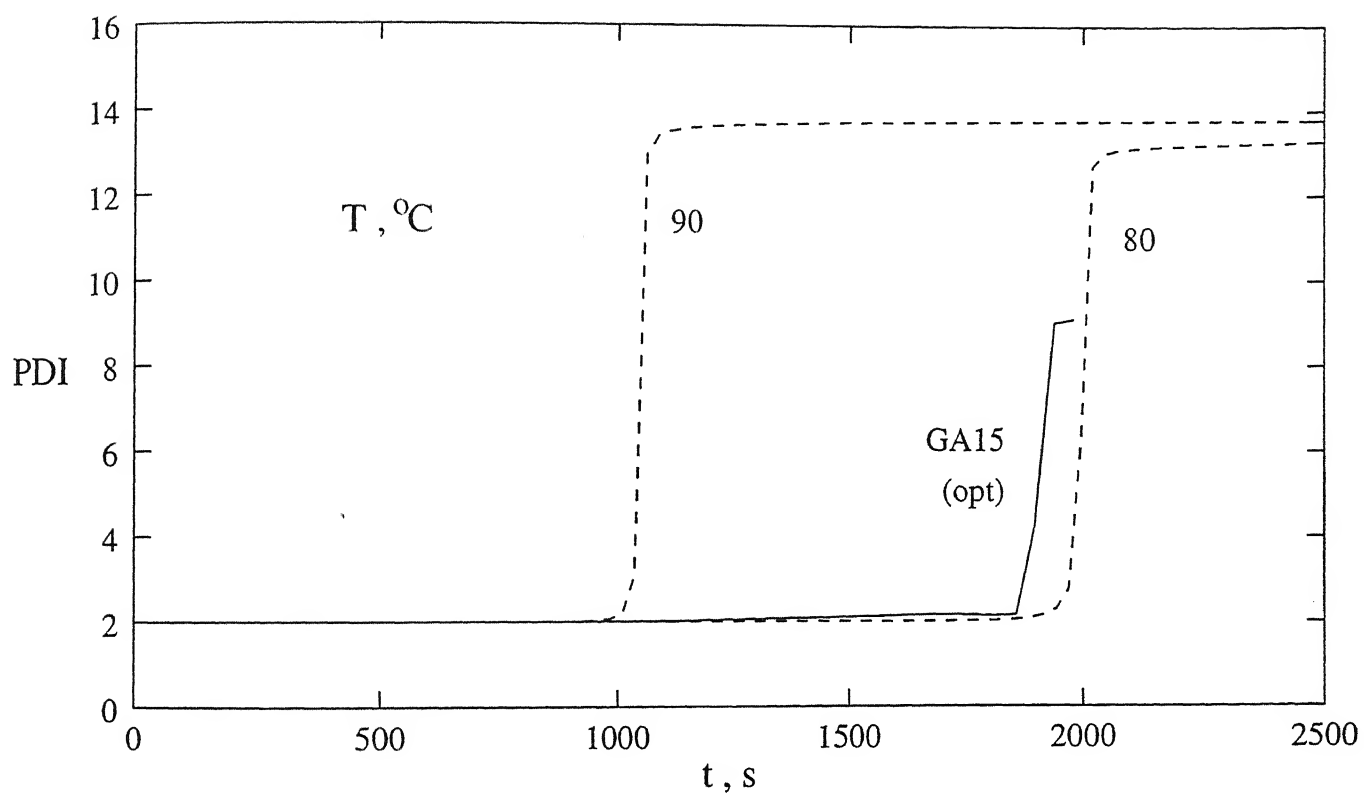


Fig. 15 : variation of the polydispersity index (PDI) with time . The solid curve represents the PDI corresponding to the GA15 run , while the dotted curves correspond to isothermal polymerizations at 80°C and 90°C .

CHAPTER 4

CONCLUSIONS

A robust optimization technique, Genetic algorithm, has been used in this study to obtain global optimal temperature histories for MMA polymerization. These can be improved further by using the first order Pontryagin method. The technique can easily be used for on-line optimizing control of experimental reactors.

ACKNOWLEDGEMENT

The authors would like to thank Professor Kalyanmoy Deb, Department of Mechanical Engineering, IIT Kanpur, for providing us the computer code, SGA, and for having several useful discussions. Also, we appreciate the partial support of this study through a grant from the Department of Science and Technology, New Delhi.

CHAPTER 5

SUGGESTIONS FOR FUTURE WORK

- (i) The rate of liquid monomer and initiator addition $R_{li}(t)$ was not considered as a control variable in the present problem. This may be included in future as a control variable along with $T(t)$ to cut down the reaction time further.
- (ii) The algorithm with proper tuning of its computational parameters can be used for on-line optimizing control of MMA polymerization process (work along these lines is in progress).

REFERENCES

- 1) V.E. Trommsdorff, H. Kohle and P. Lagally, *Makromol. Chem.*, **1**, 169 (1947).
- 2) R.G.W. Norrish and R.R. Smith, *Nature*, **150**, 336 (1942).
- 3) K.F. O'Driscoll, *Pure Appl. Chem.*, **53**, 617 (1981).
- 4) A.E. Hamielec, *Chem. Eng. Commun.*, **24**, 1 (1983).
- 5) D. Achilias and C. Kiparissides, *J. Appl. Polym. Sci.*, **35**, 1303 (1988).
- 6) D.S. Achilias and C. Kiparissides, *Macromolecules*, **25**, 3739 (1992).
- 7) I. Mita and K. Horie, *J. Macromol. Sci., Rev. Macromol. Chem. Phys.*, **C 27**, 91 (1987).
- 8) J.N. Farber in *Handbook of Polymer Science and Technology*, Vol 1, N.P. Cheremisinoff, ed., Dekker, 1989, p.429.
- 9) B.M. Louie and D.S. Soong, *J. Appl. Polym. Sci.*, **30**, 3707 (1985).
- 10) A. Faldi, M. Tirrell and T.P. Lodge, *Macromolecules*, **27**, 4176 (1994).
- 11) A. Faldi, M. Tirrell, T.P. Lodge and E. von Meerwall, *Macromolecules*, **27**, 4184 (1994).
- 12) G.T. Russell, R.G. Gilbert and D.H. Napper, *Macromolecules*, **25**, 2459 (1992).

- 13) G.T. Russell, R.G. Gilbert and D.H. Napper, *Macromolecules*, **26**, 3538 (1993).
- 14) P.A Clay and R.G. Gilbert, *Macromolecules*, **28**, 552 (1995).
- 15) W.Y. Chiu, G.M. Carratt and D.S. Soong, *Macromolecules*, **16**, 348 (1983).
- 16) G.V. Schulz and G. Harborth, *Makromol. Chem.*, **1**, 106 (1947).
- 17) S.T. Balke and A.E. Hamielec, *J. Appl. Polym. Sci.*, **17**, 905 (1973).
- 18) A.B. Ray, D.N. Saraf and S.K. Gupta, *Polym. Eng. Sci.*, **35**, 1290 (1995).
- 19) V. Seth and S.K. Gupta, *J. Polym. Eng.*, **15**, 283 (1996).
- 20) T. Srinivas, S. Sivakumar, S.K. Gupta and D.N. Saraf, *Polym. Eng. Sci.*, **36**, 311, (1996).
- 21) V. Dua, D.N. Saraf and S.K. Gupta, *Polym. Eng. Sci.*, **59**, 749 (1996).
- 22) T.J. Tulig and M.V. Tirrell, *Macromolecules*, **14**, 1501 (1981).
- 23) J.H. Holland, *Adaptation in Natural and Artificial Systems*, Univ. Michigan Press, Ann Arbor, MI, 1975.
- 24) D.E. Goldberg, *Genetic Algorithms in Search, Optimization and Machine Learning*, Addison-Wesley, MA, 1989.
- 25) K. Deb, *Optimization For Engineering Design: Algorithms and Examples*, Prentice Hall of India, New Delhi, 1995.

- 26) P.F. Lyons and A.V. Tobolsky, *Polym. Eng. Sci.*, **10**, 1 (1970).
- 27) W.H. Ray, *Advanced Process Control*, McGraw-Hill, New York, 1981; Butterworths, New York, 1989.
- 28) W.H. Ray and J.Szekeley, *Process Optimization*, Wiley, New York, 1973.
- 29) A.E. Bryson and Y.C. Ho, *Applied Optimal Control*, Blaisdell, Waltham, MA, 1969.
- 30) L. Lapidus and R. Luus, *Optimal Control of Engineering Processes*, Blaisdell, Waltham, MA, 1967.
- 31) M.E. Sachs, S. Lee and J.A. Biesenberger, *Chem. Eng. Sci.*, **27**, 2281 (1972).
- 32) J.N. Farber and R.L. Laurence, *Chem. Eng. Commun.*, **46**, 347 (1986).
- 33) S.K. Gupta, *Numerical Methods For Engineers*, New Age International Pub., New Delhi, 1995.
- 34) N.R. Vaid and S.K. Gupta, *Polym. Eng. Sci.*, **31**, 1708 (1991).
- 35) A.K. Ray and S.K. Gupta, *Polym. Eng. Sci.*, **26**, 1033 (1986).

APPENDIX A

ADDITIONAL RESULTS

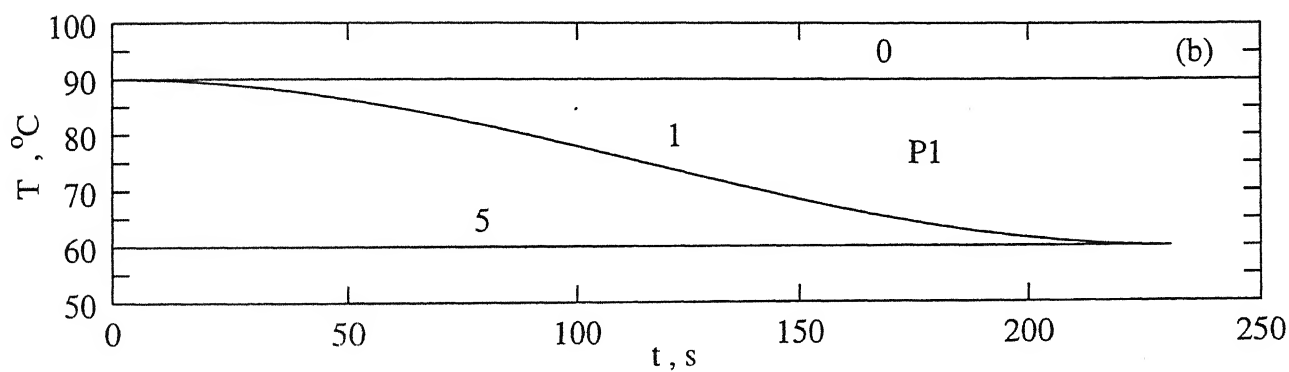
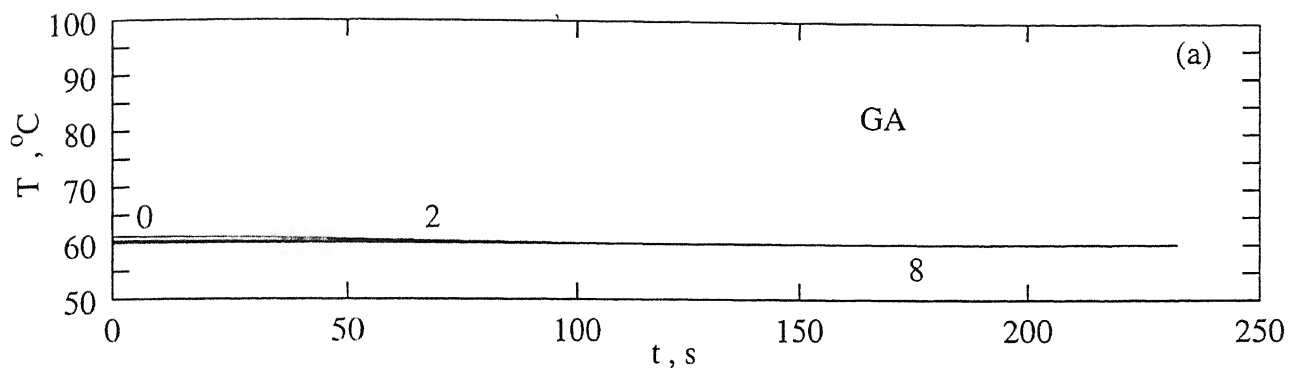


Fig. A1 : Evolution of temperature histories towards the optimal corresponding to Eq (14)

(a) using GA , generation to generation, (b) using P1 , iteration to iteration .

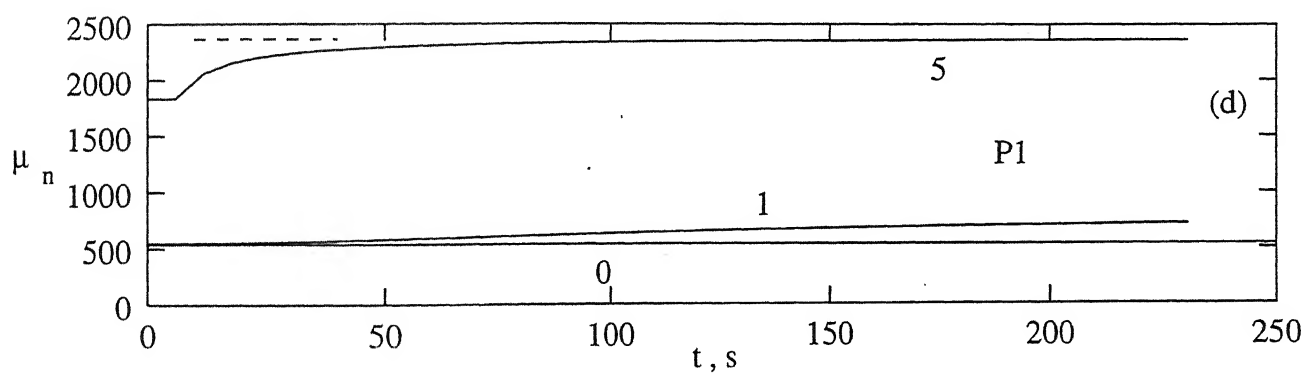
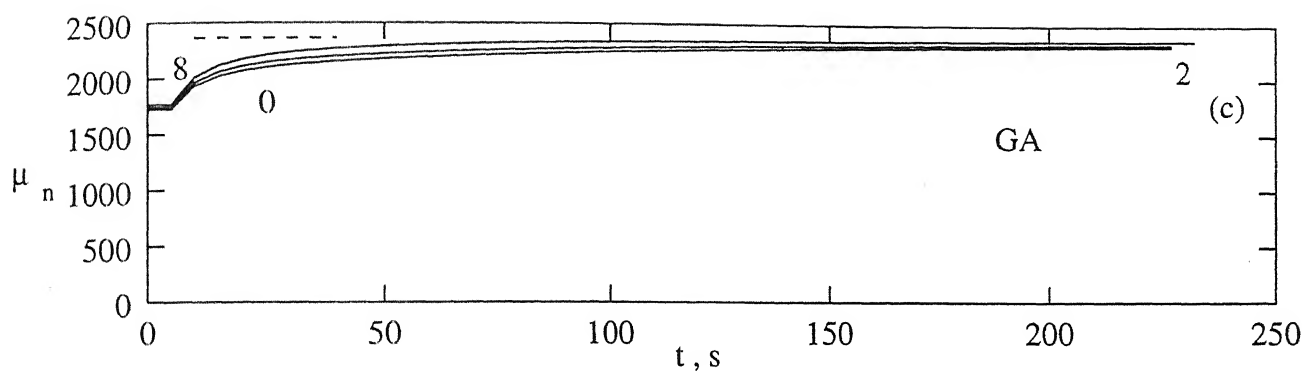


Fig. A1 : (c) , (d) $\mu_n(t)$ corresponding to temperature histories shown in Figs. (a) and (b) respectively . Dotted line indicates the desired value .

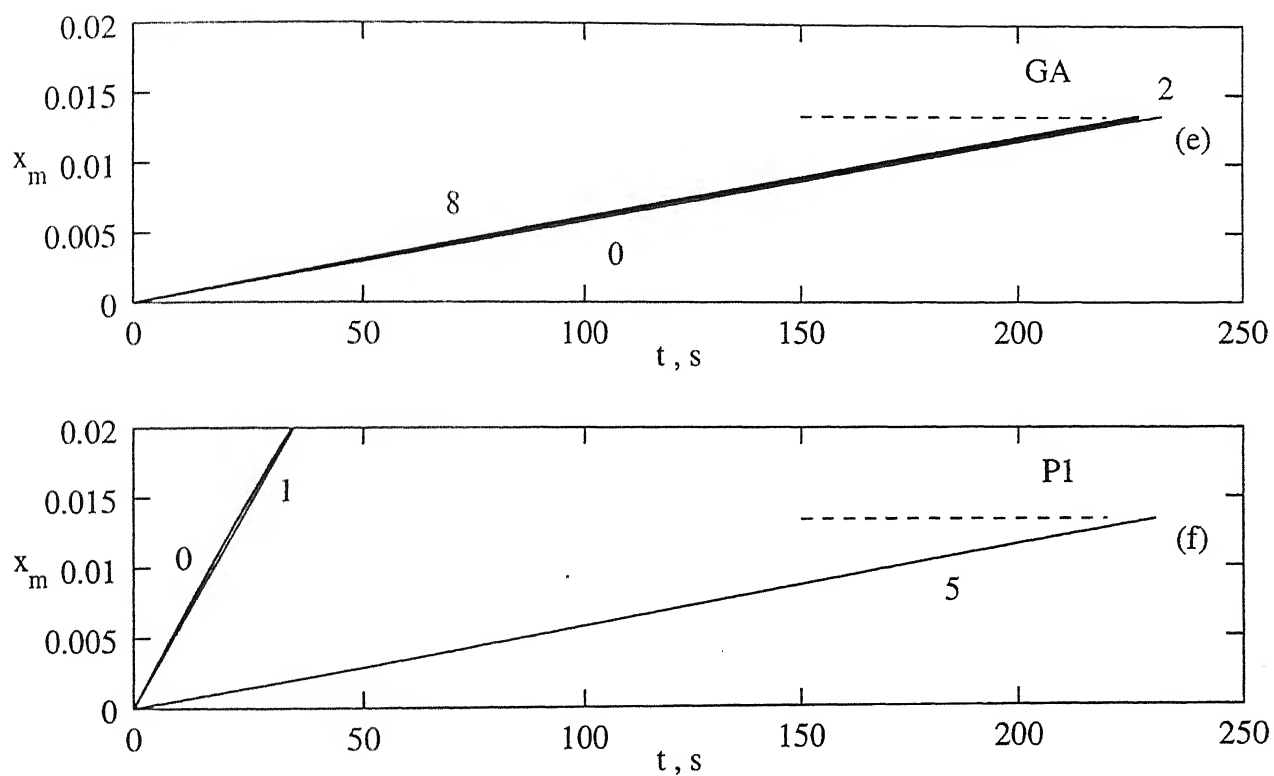


Fig. A1 : (e) , (f) $x_m(t)$ corresponding to temperature histories shown in Figs. (a) and (b) respectively . Dotted line indicates the desired values .

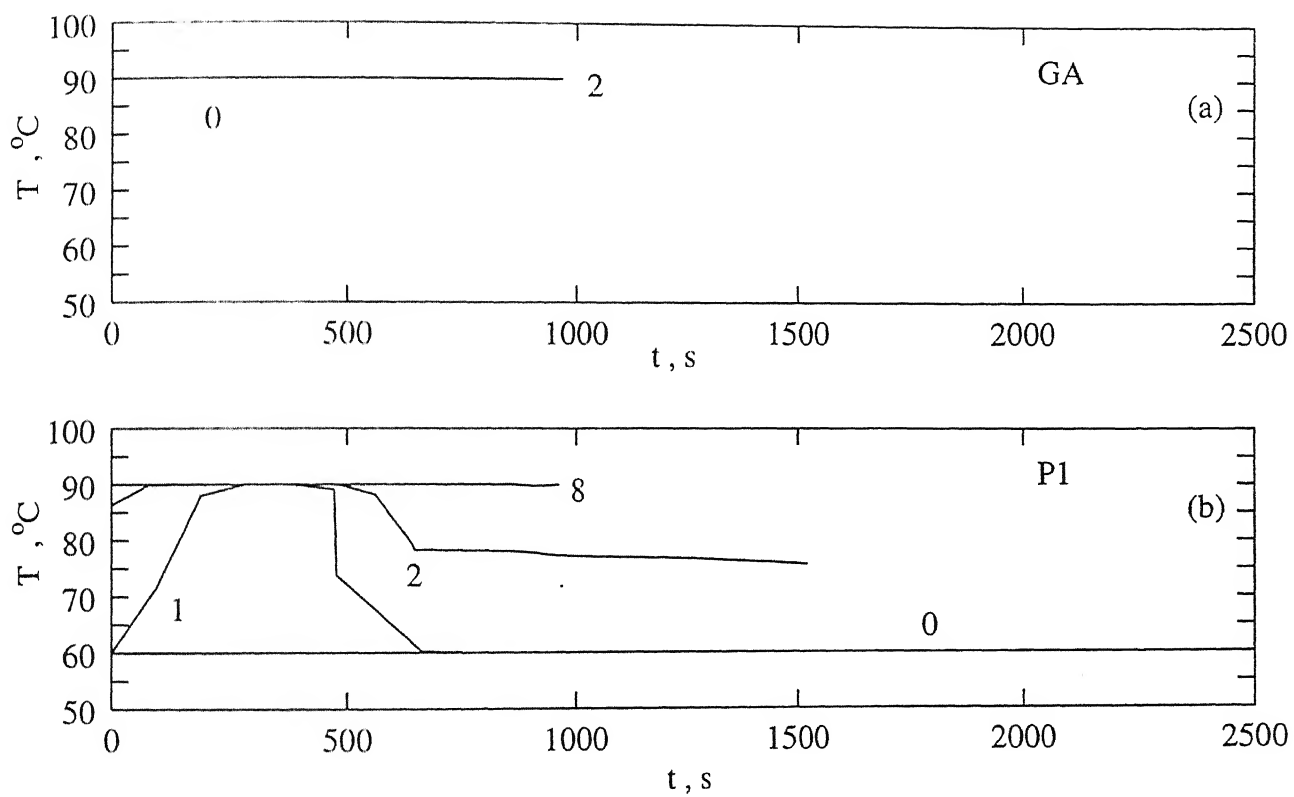


Fig. A2 : Evolution of temperature histories towards the optimal corresponding to Eq (15)
 (a) using GA , generation to generation, (b) using P1 , iteration to iteration .

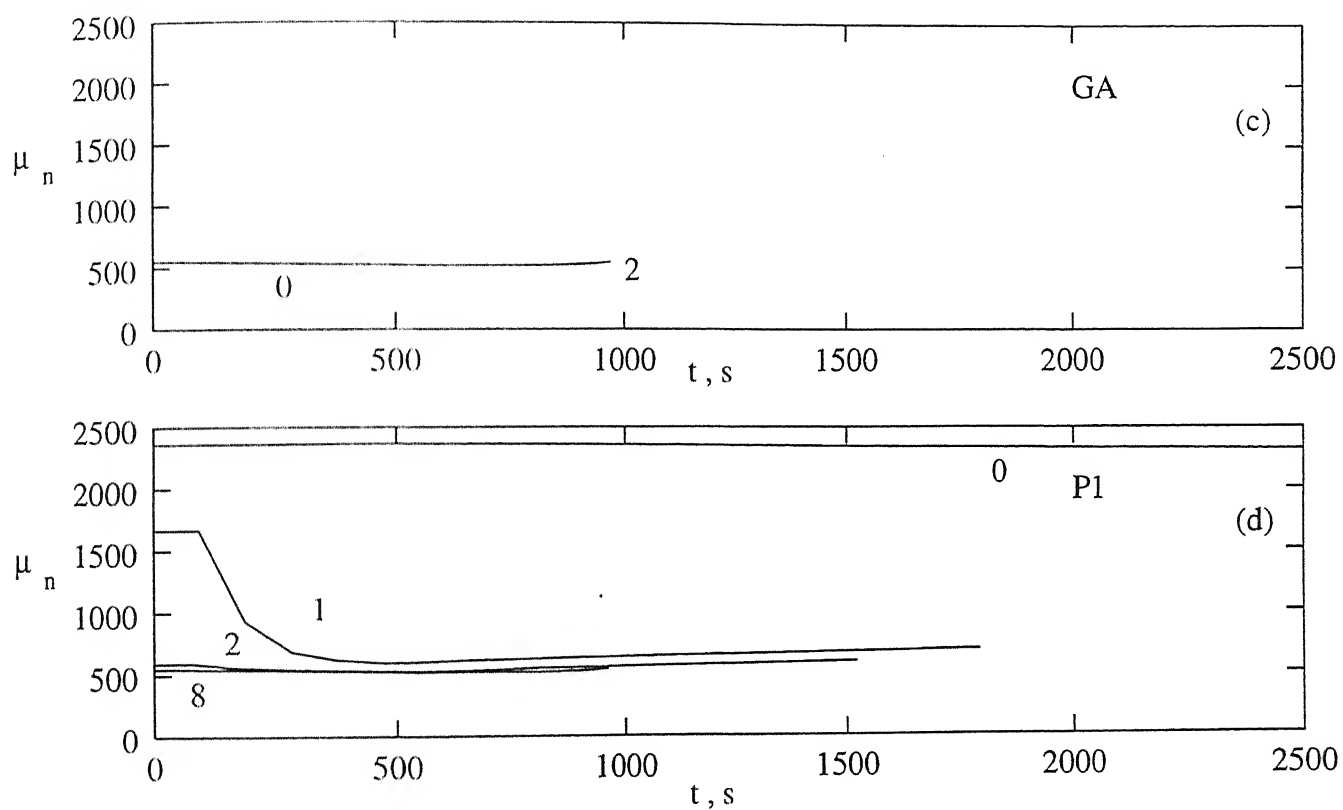


Fig. A2 : (c) , (d) $\mu_n(t)$ corresponding to temperature histories shown in Figs. (a) and (b) respectively . Dotted line indicates the desired values .

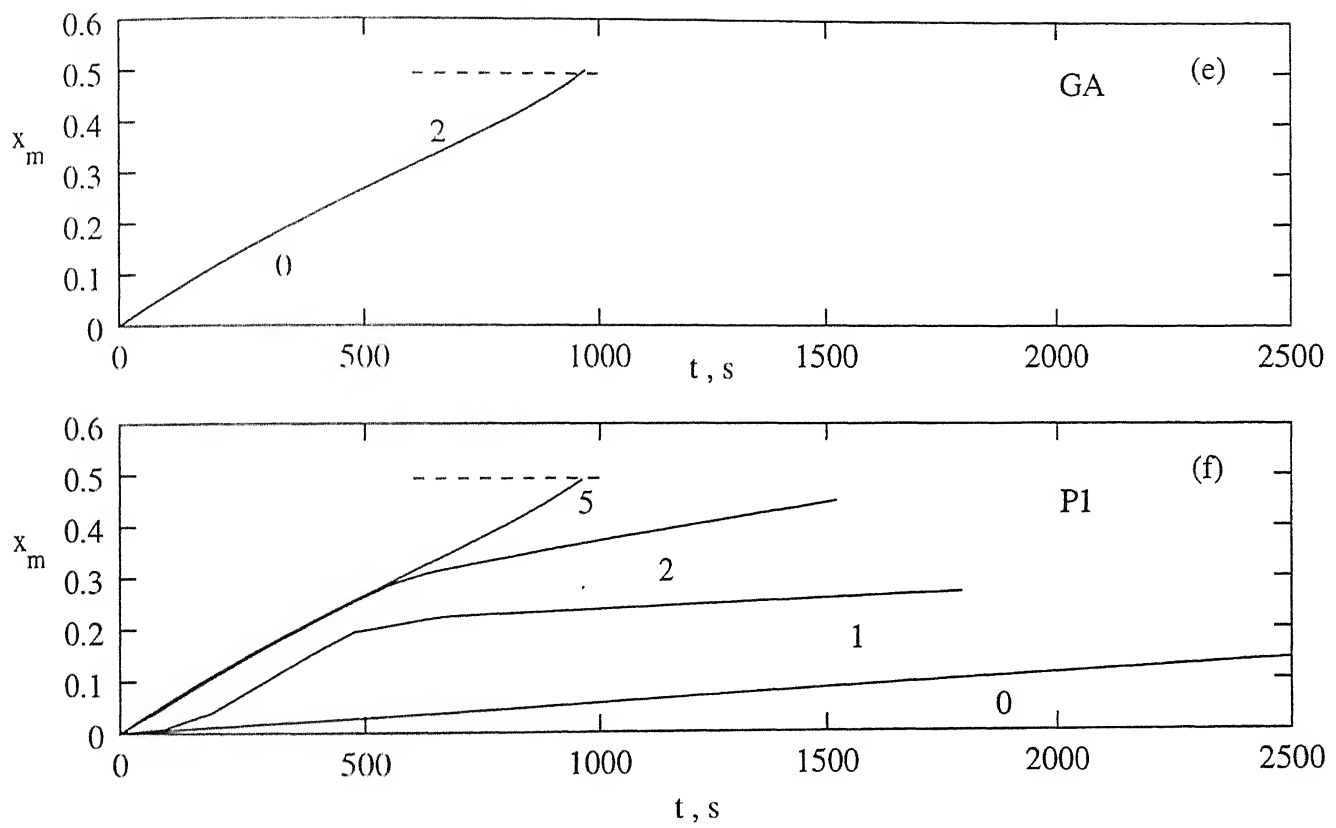


Fig. A2 : (e) , (f) $x_m(t)$ corresponding to temperature histories shown in Figs. (a) and (b) respectively . Dotted line indicates the desired values .

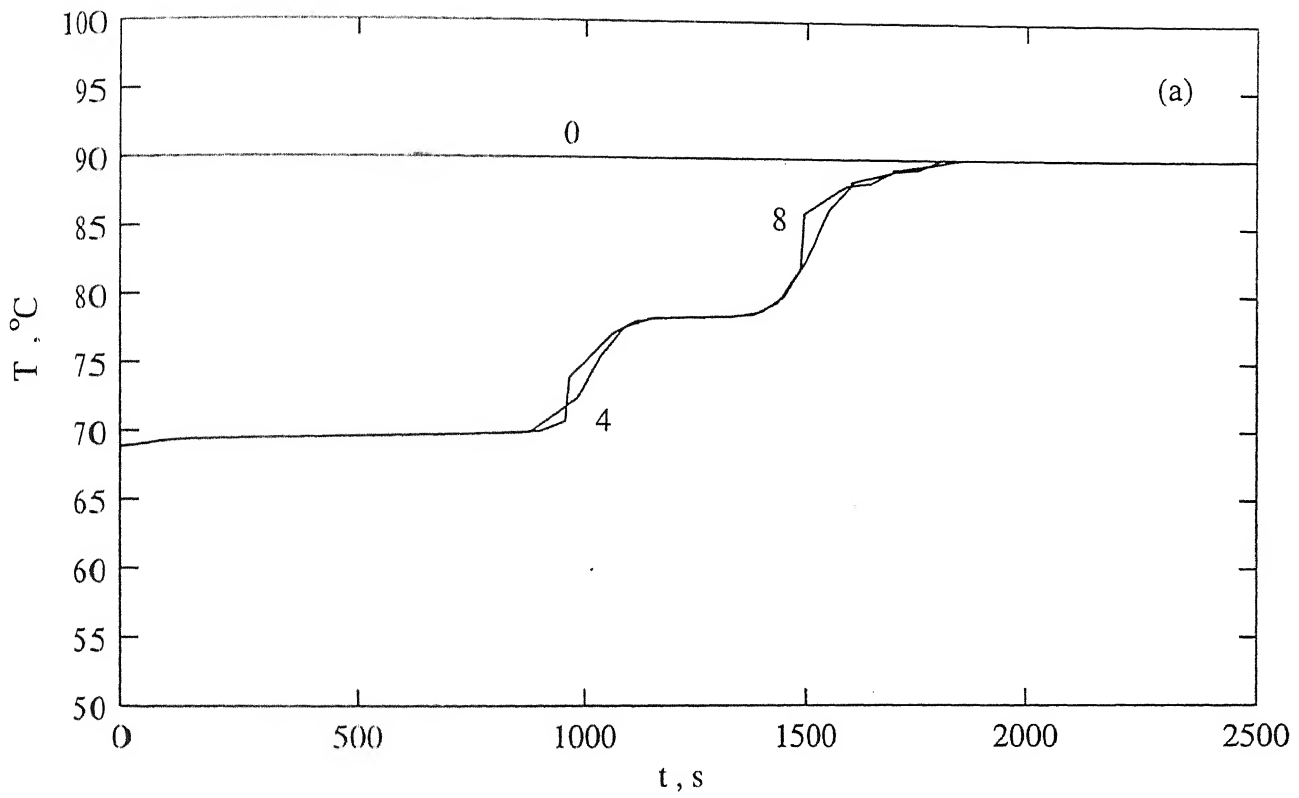


Fig.A3 : (a) Evolution of temperature histories towards the optimal corresponding to Eq (16) using PI from iteration to iteration with initial guess $T^{(0)} = 90^{\circ}\text{C}$

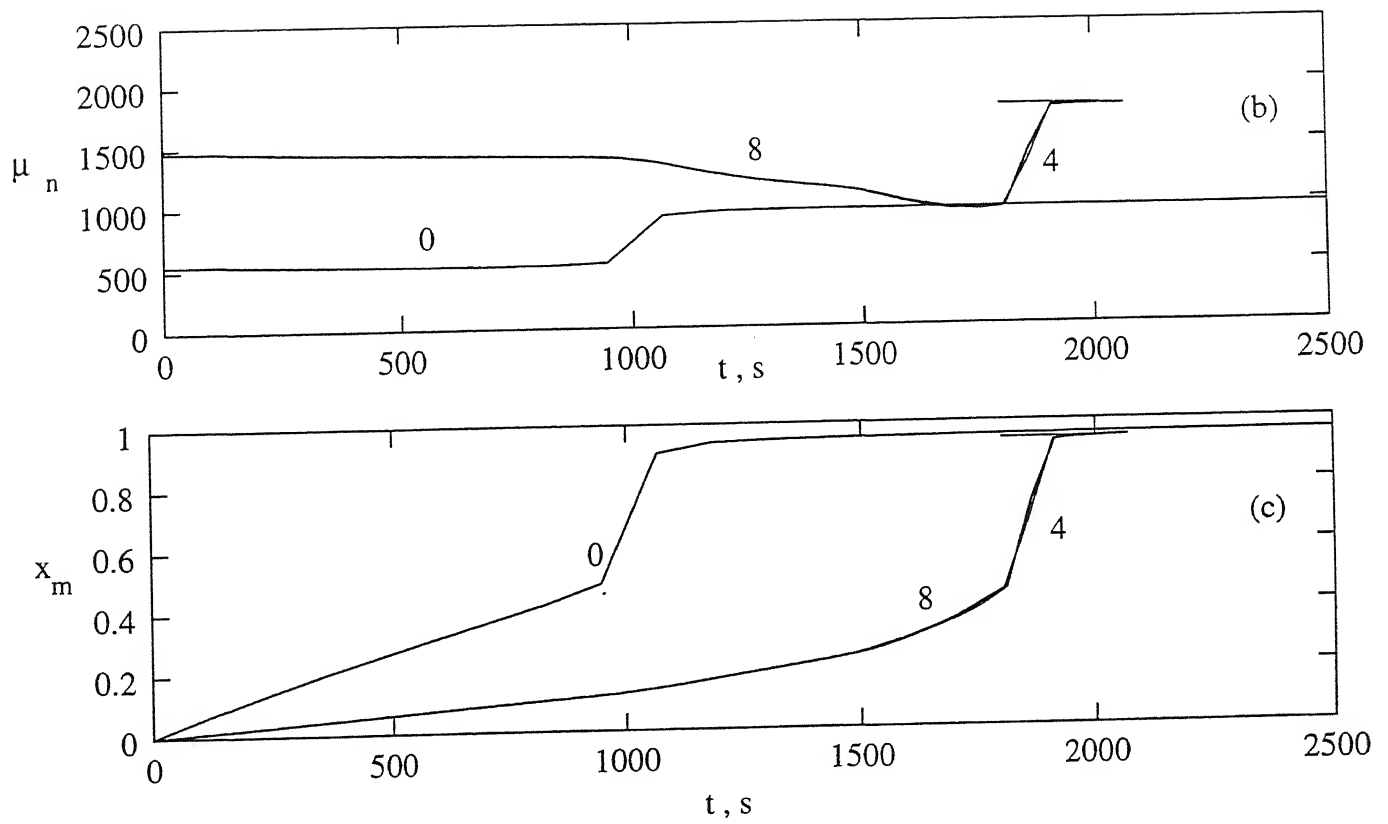


Fig. A3 : (b) , (c) $\mu_n(t)$, $x_m(t)$ corresponding to temperature histories shown in Fig. A3 (a) .
 Horizontal line (solid) indicates the desired values .

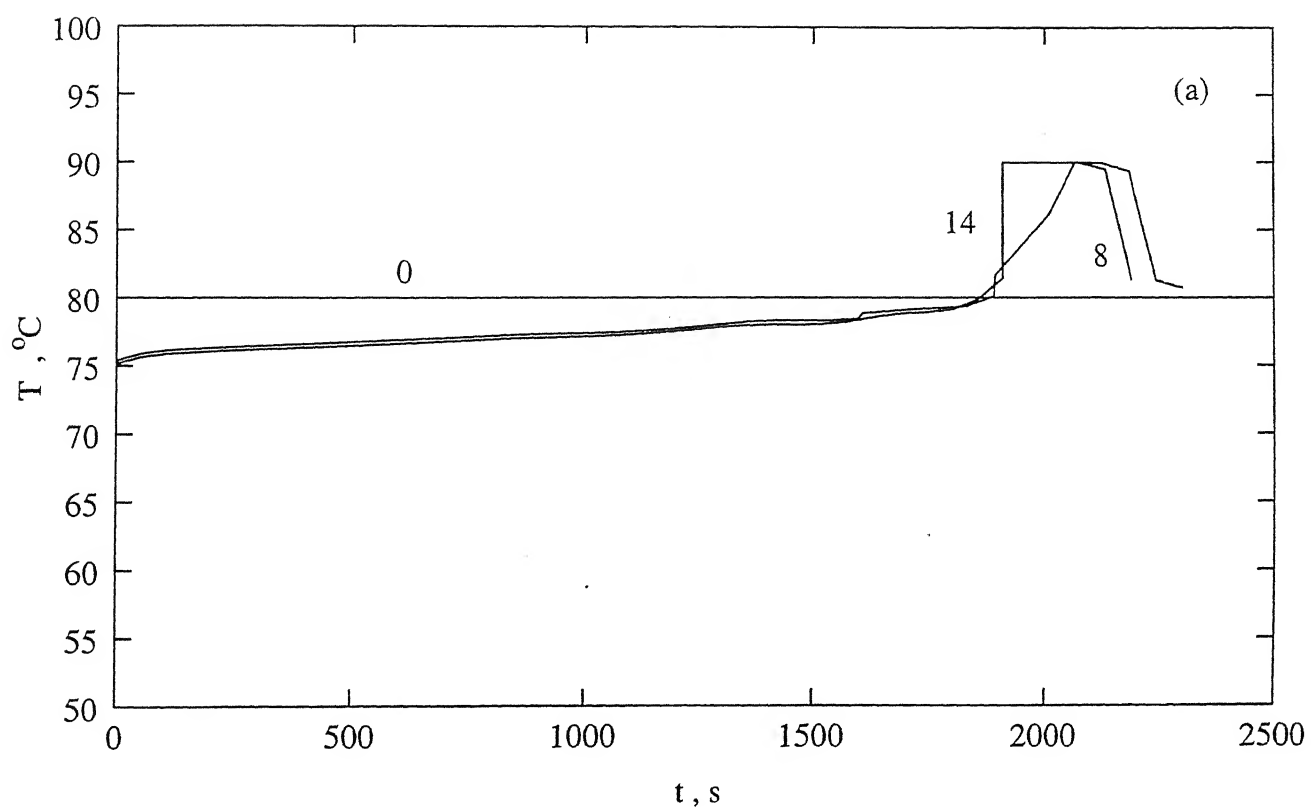


Fig. A4 : (a) Evolution of temperature histories towards the optimal corresponding to Eq (16) using P1 from iteration to iteration with initial guess $T^{(0)} = 80 \text{ }^{\circ}\text{C}$

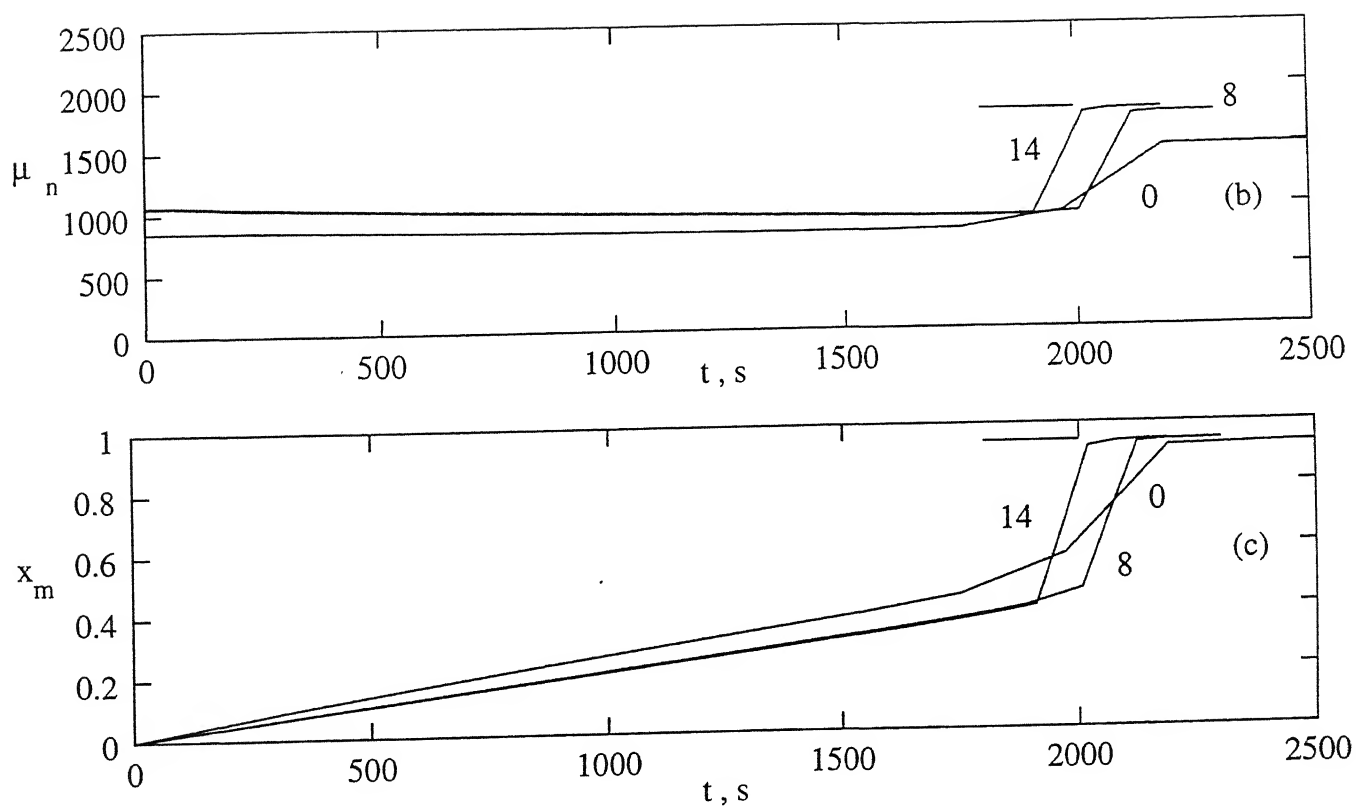


Fig. A4 : (b) , (c) $\mu_n(t)$, $x_m(t)$ corresponding to temperature histories shown in Fig. A4 (a) .
 Horizontal line (solid) indicates the desired values .

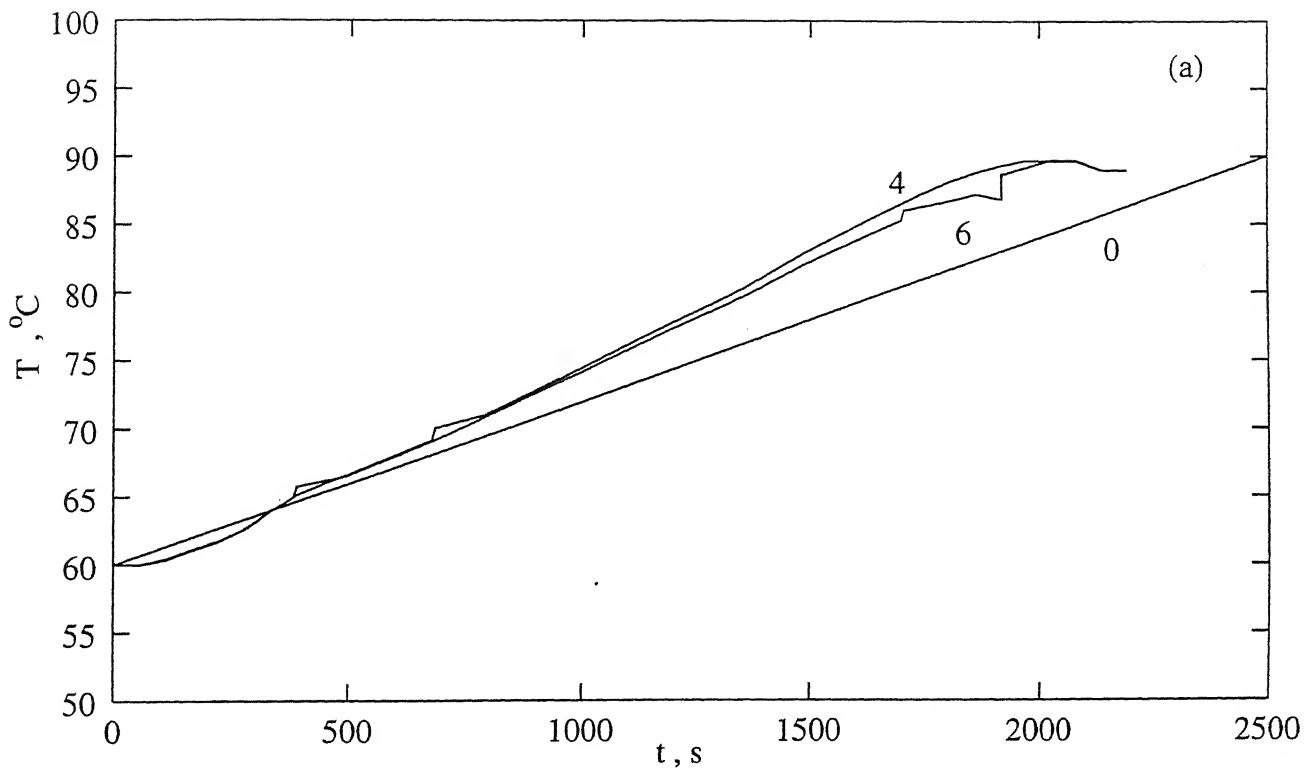


Fig. A5 : (a) Evolution of temperature histories towards the optimal corresponding to Eq(16) using P1 from iteration to iteration with initial guess $T^{(0)} =$ linear profile from 60 - 90 °C .

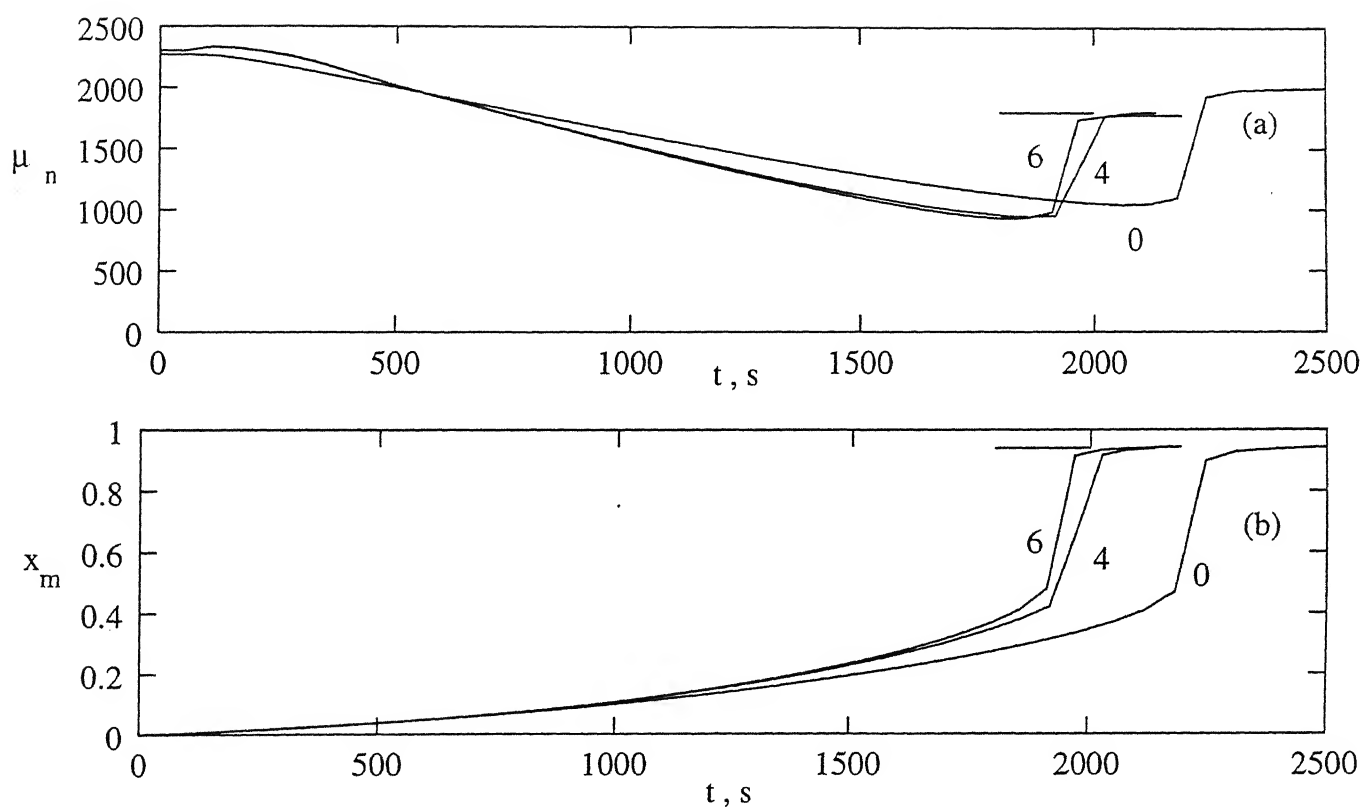


Fig. A5 : (b), (c) $\mu_n(t)$, $x_m(t)$ corresponding to temperature histories shown in Fig. A5 (a) .

Horizontal line (solid) indicates the desired values .

APPENDIX B
ADDITIONAL TABLES

TABLE B1

MODEL EQUATIONS FOR MMA POLYMERIZATION IN SEMIBATCH REACTORS¹⁹

$$1. \quad \frac{dI}{dt} = -k_d I + R_{li}(t)$$

$$2. \quad \frac{dM}{dt} = - (k_p + k_f) \frac{\lambda_o M}{V_1} - k_i \frac{R M}{V_1} - k_s S \frac{\lambda_o}{V_1} \\ + R_{lm}(t) - R_{vm}(t)$$

$$3. \quad \frac{dR}{dt} = 2fk_d I - k_i \frac{R M}{V_1}$$

$$4. \quad \frac{dS}{dt} = R_{ls}(t) - R_{vs}(t)$$

$$5. \quad \frac{d\lambda_o}{dt} = k_i \frac{R M}{V_1} - k_t \frac{\lambda_o^2}{V_1}$$

$$6. \quad \frac{d\lambda_1}{dt} = k_i \frac{R M}{V_1} + k_p M \frac{\lambda_o}{V_1} - k_t \frac{\lambda_o \lambda_1}{V_1} \\ + (k_s S + k_f M) \frac{(\lambda_o - \lambda_1)}{V_1}$$

$$7. \quad \frac{d\lambda_2}{dt} = k_i \frac{R M}{V_1} + k_p M \frac{\lambda_o + 2\lambda_1}{V_1} - k_t \frac{\lambda_o \lambda_2}{V_1} \\ + (k_s S + k_f M) \frac{(\lambda_o - \lambda_2)}{V_1}$$

$$8. \quad \frac{d\mu_o}{dt} = (k_s S + k_f M) \frac{\lambda_o}{V_1} + (k_{td} + \frac{1}{2}k_{tc}) \frac{\lambda_o^2}{V_1}$$

Contd... b

Table B1 (Contd... b)

$$9. \quad \frac{d\mu_1}{dt} = (k_s S + k_f M) \frac{\lambda_1}{V_1} + k_t \frac{\lambda_o \lambda_1}{V_1}$$

$$10. \quad \frac{d\mu_2}{dt} = (k_s S + k_f M) \frac{\lambda_2}{V_1} + k_t \frac{\lambda_o \lambda_2}{V_1} + k_{tc} \frac{\lambda_1^2}{V_1}$$

$$11. \quad \frac{d\xi_m}{dt} = R_{lm}(t) - R_{vm}(t)$$

$$12. \quad \frac{d\xi_{m1}}{dt} = R_{lm}(t)$$

$$13. \quad V_1 = \frac{S (MW_s)}{\rho_s} + \frac{M (MW_m)}{\rho_m} + \frac{(\xi_m - M) (MW_m)}{\rho_p}$$

$$14. \quad \phi_m = \frac{M (MW_m) / \rho_m}{\frac{M (MW_m)}{\rho_m} + \frac{S (MW_s)}{\rho_s} + \frac{(\xi_m - M) (MW_m)}{\rho_p}}$$

$$15. \quad \phi_s = \frac{S (MW_s) / \rho_s}{\frac{M (MW_m)}{\rho_m} + \frac{S (MW_s)}{\rho_s} + \frac{(\xi_m - M) (MW_m)}{\rho_p}}$$

$$16. \quad \phi_p = 1 - \phi_m - \phi_s$$

TABLE B2

CAGE, GEL AND GLASS EFFECT EQUATIONS¹⁹

$$\frac{1}{f} = \frac{1}{f_o} \left[1 + \theta_f(T) \frac{M}{V_1} \frac{1}{\exp \left[\xi_{13} \left\{ -\psi + \psi_{\text{ref}} \right\} \right]} \right] \quad (\text{a})$$

$$\frac{1}{k_t} = \frac{1}{k_{t,o}} + \theta_t(T) \mu_n^2 \frac{\lambda_o}{V_1} \frac{1}{\exp \left[-\psi + \psi_{\text{ref}} \right]} \quad (\text{b})$$

$$\frac{1}{k_p} = \frac{1}{k_{p,o}} + \theta_p(T) \frac{\lambda_o}{V_1} \frac{1}{\exp \left[\xi_{13} \left\{ -\psi + \psi_{\text{ref}} \right\} \right]} \quad (\text{c})$$

$$\psi = \frac{\gamma \left\{ \frac{\rho_m \phi_m \hat{V}_m^*}{\xi_{13}} + \frac{\rho_s \phi_s \hat{V}_s^*}{\xi_{23}} + \rho_p \phi_p \hat{V}_p^* \right\}}{\rho_m \phi_m \hat{V}_m^* V_{fm} + \rho_s \phi_s \hat{V}_s^* V_{fs} + \rho_p \phi_p \hat{V}_p^* V_{fp}} \quad (\text{d})$$

$$\psi_{\text{ref}} = \frac{\gamma}{V_{fp}} \quad (\text{e})$$

$$\xi_{13} = \frac{\hat{V}_m^* (MW_m)}{\hat{V}_p^* M_{jp}} \quad (\text{f})$$

$$\xi_{23} = \frac{\hat{V}_s^* (MW_s)}{\hat{V}_p^* M_{jp}} \quad (\text{g})$$

Contd.... b

Table B2 (Contd... b)

$$\xi_{I3} = \frac{\hat{V}_I^* (MW_I)}{\hat{V}_p^* M_{jp}} \quad (h)$$

$$k_d = k_d^0 \exp (-E_d/RT) \quad (i)$$

$$k_{p,o} = k_{p,o}^0 \exp (-E_p/RT) \quad (j)$$

$$k_{t,o} = k_{td,o} = k_{td,o}^0 \exp (-E_{td}/RT) \quad (k)$$

TABLE B3
PARAMETERS USED FOR POLYMERIZATION OF
MMA¹⁹

| | | |
|--------------------|---|--|
| ρ_m | = | 966.5 - 1.1 (T - 273.1) kg/m ³ |
| ρ_p | = | 1200 kg/m ³ |
| ρ_s | = | 844.18 - 1.07165 (T - 323.1) kg/m ³ (Benzene) |
| f_o | = | 0.58; for AIBN |
| k_d^o | = | 1.053x10 ¹⁵ s ⁻¹ ; for AIBN |
| $k_{p,o}^o$ | = | 4.917x10 ² m ³ /mol-s |
| $k_{td,o}^o$ | = | 9.8x10 ⁴ m ³ /mol-s |
| k_{tc} | = | 0.0 |
| k_f | = | 0.0 |
| k_i | = | k_p |
| k_s | = | 0.0 |
| E_d | = | 128.45 kJ/mol ; for AIBN |
| E_p | = | 18.22 kJ/mol |
| E_{td} | = | 2.937 kJ/mol |
| (MW _m) | = | 0.10013 kg/mol |
| (MW _s) | = | 0.07811 kg/mol |

Contd... b

Table B3 (Contd... b)

(MW_I) = 0.06800 kg/mol; for radicals from AIBN

Constitutive Parameters for the Cage, Gel and Glass Effects

$$\begin{aligned}\hat{V}_I^* &= 9.13 \times 10^{-4} \text{ m}^3/\text{kg}; && \text{for AIBN} \\ \hat{V}_m^* &= 8.22 \times 10^{-4} \text{ m}^3/\text{kg} \\ \hat{V}_p^* &= 7.70 \times 10^{-4} \text{ m}^3/\text{kg} \\ M_{jp} &= 0.18781 \text{ kg/mol} \\ \gamma &= 1 \\ V_{fm} &= 0.149 + 2.9 \times 10^{-4} [T(K) - 273.1] \\ V_{fp} &= 0.0194 + 1.3 \times 10^{-4} [T(K) - 273.1 - 105]; \\ &&& \text{for } T < (105 + 273.1) \text{ K}\end{aligned}$$

Correlations used for θ_f , θ_p , θ_t ¹⁹

$$\log_{10} [10^3 \theta_f(T), \text{ m}^3 \text{ mol}^{-1}] = 2.016 \times 10^2 - 1.455 \times 10^5 (1/T) + 2.70 \times 10^7 (1/T^2)$$

$$\log_{10} [\theta_p(T), \text{ s}] = 8.03 \times 10^1 - 7.50 \times 10^4 (1/T) + 1.765 \times 10^7 (1/T^2)$$

$$\log_{10} [\theta_t(T), \text{ s}] = 1.241 \times 10^2 - 1.0314 \times 10^5 (1/T) + 2.2735 \times 10^7 (1/T^2)$$

APPENDIX C
COMPUTER PROGRAMS